Title: Biological sex-dependent hormonal signaling and metabolomic profiles in obesity alter tumor microenvironment and immunotherapy outcomes

Logan V. Vick[1,2], Spencer R. Rosario[3] Ziming Wang[1±], Craig Collins[1], Lam T. Khuat[1±], Yatian Yang[5], Michael Sheng[1], Wahed A. Firoz[1], Ryan Nielsen[1], Yao-Hui Sun[2], Aryana M. Razmara[6], Hossein Borghaei[7], Emmanuel S. Antonarakis[8], Andrew Elliott[5], Nishant Gandhi[5], Raid Aljumaily[9], Sami Ibrahimi[9], Michael Machiorlatti[10], Sara K. Vesely[10], Shuchi Gulati[11], Sarbajit Mukherjee[12], Robert J. Canter[6], Sean J. Judge[6], Arta M. Monjazeb[2§] and William J. Murphy[1,13§*].

1. Department of Dermatology, University of California Davis School of Medicine, Sacramento, CA, USA.
2. Department of Radiation Oncology, University of California Davis Comprehensive Cancer Center, University of California School of Medicine, Sacramento, CA, USA
3. Department of Biostatistics and Bioinformatics, Roswell Park Comprehensive Cancer Center, Buffalo, New York, USA
4. Antibody and Vaccine Group, Centre for Cancer Immunology, School of Cancer Sciences, Faculty of Medicine, Southampton General Hospital, University of Southampton, Southampton, United Kingdom.
5. Caris Life Sciences, Phoenix, AZ
6. Department of Surgery, Division of Surgical Oncology, University of California Davis Comprehensive Cancer Center, University of California Davis School of Medicine, Sacramento, CA, USA.
7. Department of Hematology and Oncology, Fox Chase Cancer Center, Philadelphia, Pennsylvania
8. Masonic Cancer Center, University of Minnesota-Twin Cities, Minneapolis, Minnesota
9. Department of Internal Medicine, Section of Hematology and Oncology, University of Oklahoma Health Sciences Center, Oklahoma City, OK, USA
10. Department of Biostatistics and Epidemiology, University of Oklahoma Health Sciences Center, Oklahoma City, OK, USA
11. Department of Internal Medicine, Division of Hematology/Oncology, University of California Davis School of Medicine and the UC Davis Comprehensive Cancer Center, Sacramento, CA, USA
12. Department of Medical Oncology, Miami Cancer Institute, Baptist Health South Florida, Miami, FL, U.S.A.5.
13. Department of Internal Medicine, Division of Malignant Hematology, Cell and Tissue Transplantation, University of California Davis School of Medicine, Sacramento, CA, USA.

±Current affiliation: Ziming Wang, Immuno-Oncology Cell Therapy, Janssen Oncology, Spring House, PA, United States

§These authors jointly supervised this work: William J. Murphy, Arta M. Monjazeb

*Corresponding Author: Dr. William J. Murphy, Distinguished Professor,

Abstract

Commonly viewed as a negative prognostic factor in cancer, obesity is associated with improved responses to cancer immunotherapy using immune checkpoint inhibitors (ICIs). Although data suggest a sexual dimorphism influencing the effects of obesity on immunotherapy responses, to our knowledge, the intersection of sex and obesity on immunotherapy requires further exploration. We demonstrate, in a pan-cancer analysis stratified by sex and BMI, that obesity (BMI ≥ 30) is associated with improved survival after ICI only in male patients. In preclinical models of diet-induced obesity (DIO), we observed that only DIO male tumor-bearing mice responded better to ICI. The differential effect of sex on outcomes was associated with alterations in the tumor microenvironment where DIO female mice demonstrated increased tumor-associated macrophages skewed toward a M2 phenotype. Ovariectomy of DIO female mice reduced M2 polarization and increased anti-tumor immune responses including increases in tumor-infiltrating T cells following ICI. Metabolomic analysis of DIO mice demonstrated distinct profiles base on sex. Re-stratification of female cancer patients revealed that obesity was associated with improved outcome, but only in post-menopausal (age ≥ 55) patients. We identify that the immunotherapy “obesity paradox” is sex-dependent and that hormonal and metabolomic status modulates the influence of obesity on ICIs.

Introduction

Immune checkpoint inhibitors (ICIs) have improved outcomes for patients across multiple malignancies, including melanoma, non-small cell lung cancer (NSCLC), renal cell carcinoma (RCC), and others (1). Although responses can be potent, patient selection and risk stratification need improvement. Biomarkers including PD-L1 expression (2, 3), tumor mutational burden (TMB) (3, 4), and microsatellite instability-high (MSI-H) status (5, 6) have reproducibly been associated with greater ICI efficacy. Evidence has demonstrated that patient parameters, including microbiome and obesity predict ICI response (7).

The epidemic of obesity has garnered attention due to the global increases in the number of individuals categorized as either overweight or obese, and the increasing incidence of obesity related morbidity and mortality in cancer and other diseases (8, 9). Obesity is characterized by increased adiposity, associated with low-grade inflammation, and linked to metabolic disorders (e.g., diabetes, non-alcoholic fatty liver disease, metabolic syndrome, etc.) (7, 8, 10–12). Clinically, a body mass index (BMI) ≥ 30 defines obesity although there are limitations to using BMI alone (11, 13–16).

Despite the known associations of obesity with cancer incidence and adverse clinical outcomes (17–21), obesity is associated with improved response to ICIs, a phenomenon referenced as “the obesity paradox” (22–37). The positive association of obesity with ICI efficacy is still not completely understood as the “paradox” has not always been observed (38–42).

The role of biologic sex on obesity is also complex. Studies have observed sex-based differences in ICI responses among obese patients, most notably in melanoma. An analysis by McQuade et al. (2018) (22), demonstrate that the greatest benefit to ICI is among obese male patients (22, 26, 43). Few studies have explored this apparent sex-based difference in immunotherapy responses, although studies have identified that hormones including estrogens and androgens can markedly impact cancer, immunity, and immunotherapy (44–51).

We sought to evaluate the immunomodulatory role of biologic sex on ICI efficacy in obese subjects using clinical data and interrogated the interaction of sex and obesity in pre-clinical models and human biospecimens. We corroborate previous findings that obesity is associated with improved ICI response clinically and demonstrate that this effect is most pronounced in obese male patients. Mirroring our clinical data, diet induced obese (DIO) male and female mice exhibit differences in response to ICI with female obese mice failing to respond to ICI. Mechanistically, DIO female mice display increases in tumor associated macrophages (TAMs) with increased M2 polarization contributing to immune suppression and ICI resistance. Importantly, the effects of ICIs were augmented in DIO female mice through prior ovariectomy, restoring ICI efficacy comparable to DIO males. We identified key distinctions in the metabolomic profile between DIO males and females as well as metabolite profiles linked to ICI anti-tumor efficacy. Stratification of female cancer patients treated with ICIs based on age, a surrogate for menopausal status, revealed that obesity for older and not younger female patients was associated with improved ICI responses. Our data indicate that hormonal signaling in obesity impacts ICI outcomes and suggests potential strategies for identification of ICI receptivity.

Results

Obesity is associated with better outcomes in male, but not female patients receiving immune checkpoint inhibitors. Although an association between obesity and ICI response is reported, this association and the underlying mechanisms driving improved outcome remain controversial (52). In a pan-cancer assessment of patients treated with ICIs (anti-PD-1/PD-L1) stratified by BMI less than and greater than 30, we previously reported that patients with a BMI ≥30 had significantly increased progression free survival (PFS) and overall survival (OS) (24). Given previous evidence (22, 26, 43) which identified that patient sex may influence ICI outcomes in obese patients, we analyzed the role of sex-dependent differences in immunotherapy response. We stratified pan-cancer OS and PFS data from Wang et al (2019) (24) by BMI (≥30 or <30) and patient sex. From 250 cancer patients, treated with anti-PD-1/L1 ICIs, 114 were male and 136 female (Supplemental Table 1). Multivariate analysis

incorporating age, sex, ECOG, BMI, stage and cancer type was performed for OS (HR = 0.61; 95% CI: 0.39 -0.94) and PFS (HR = 0.63; 95% CI: 0.43 -0.94) (Supplemental Table 2 & 3). Male patients with BMI ≥ 30 experienced significantly improved OS and PFS compared to male patients with BMI <30 (Figure 1A-B). No significant difference in OS or PFS was observed using the same comparison in female patients (Figure 1C-D). In a direct comparison of obese male and female patients we observed no significant difference in OS or PFS, yet non-obese female patients did demonstrate significantly better OS then non-obese male patients with no difference observed in PFS (Supplemental Figure 1A-F). These data corroborate an association of improved oncologic outcomes among obese patients undergoing ICI and highlights the interaction of patient sex on these outcomes.

To validate our findings in a larger patient cohort in distinct cancer types, we utilized data from Caris Life Sciences investigating the two most abundant cancer types in our dataset: melanoma and lung. Stratification by BMI and sex on a larger melanoma patient cohort treated with ICI demonstrated significant improvement in survival of male patients with BMI ≥ 30 when compared with those with BMI < 30; female patients with high BMI did not demonstrate this benefit (Supplemental Figure 2A-B). Evaluation of patients with non-small cell lung cancer (NSCLC) yielded more mixed results. High BMI (BMI ≥ 30) male NSCLC-Adenocarcinoma patients but not females demonstrated improved survival when compared to their respective low BMI (BMI< 30) counterparts (Supplemental Figure 2C-D). However, both high BMI male and female NSCLC-Squamous patients demonstrated a significant improvement in survival (Supplemental Figure 2E-F). These data illustrate a BMI and sex dependent response to ICI suggesting that the obesity paradox in the context of sex requires further investigation.

Male but not female DIO mice demonstrate decreased tumor burden and improved anti-tumor responses following anti-PD-1 immunotherapy. We next aimed to delineate the role of biologic sex in immunotherapy responses in pre-clinical models of obesity and cancer. We utilized a DIO model consistent with prior studies (24, 53–55) placing both male and female mice on a regimen of either a 10% fat control diet or a high fat diet (HFD) consisting of 60% fat by lard (Supplemental Figure 3A-C)

(24, 53). Studies have identified female mice as more resistant to DIO than male counterparts manifested by reduced weight gain and resistance to metabolic disorders (56, 57). Here, we observed that both male and female mice placed on HFD achieved significantly increased bodyweight gain when compared to age matched controls on a 10% fat diet as early as two months after starting diet (Figure 2A). When fed HFD male mice demonstrated an increased rate of weight gain initially when compared to female mice (Supplemental Figure 3D), yet after four months both male and female mice demonstrated comparable bodyweight (Figure 2A). Both male and female DIO mice developed increased adiposity demonstrated by MRI imaging (Figure 2B) accompanied by significantly elevated serum leptin levels (Supplemental Figure 3E) compared to lean counterparts. Female DIO mice had significantly higher leptin levels than DIO males. Both male and female DIO mice had elevated levels of resting serum glucose when compared to control diet counterparts (Supplemental Figure 3F). Neither male nor female DIO mice demonstrated increased levels of hemoglobin A1c when compared to lean controls (Supplemental Figure 3G).

To evaluate baseline differences in immunity, we performed flow cytometry on the peripheral blood of control and DIO mice assessing immune cell composition and phenotype (Supplemental Figure 4A-B). We observed that DIO female mice had a significantly higher myeloid compartment in the blood when compared to lean counterparts and reciprocally demonstrated significantly decreased T and NK cells (Supplemental Figure 4C-F). We have previously reported that aged mice on diet have significant increases in the percentage of PD-1+ and memory T cell compartments in tissues such as liver (24) and blood (53), but we did not observe any significant differences in the peripheral blood at this younger age (Supplemental Figure 5A-E).

To assess response to anti-PD-1 ICIs using both male and female mice, we utilized two syngeneic tumor lines, B16F0 melanoma and Lewis lung carcinoma (3LL) (Figure 2C). Tumors progressed faster in untreated DIO mice with both tumor lines regardless of sex (Supplemental Figure 6A-C). Anti-PD-1 treated DIO male mice had a significant decrease in tumor burden in both models. However, we did not observe a significant difference in the reduction of tumor burden in DIO female,

lean female, or lean male mice following treatment (Figure 2D-G, Supplemental Figure 4D). In representative studies, DIO male mice demonstrated robust anti-tumor responses in 4/6 mice challenged with B16F0 (Figure 2H) and 9/10 challenged 3LL (Figure 2I) while responses were muted for all other groups. Similarly, B16F0 survival studies demonstrate that only DIO male mice treated with anti-PD-1 have significantly improved survival over untreated controls (Supplemental Figure 6E-J).

Sectioned tumors stained with hematoxylin and eosin (H&E) revealed increased necrosis in all melanoma samples as well as the presence of increased adipocytes within the tumor tissue of DIO mice in both tumor types (Supplemental Figure 7A-B). These data illustrate that the DIO environment contributes to more rapid tumor growth regardless of sex while only DIO male mice respond to anti-PD-1 immunotherapy.

Obesity differentially modulates the tumor microenvironment based on biologic sex promoting increased M2 tumor associated macrophages in DIO female mice. Obesity is characterized by immune dysfunction and immune suppression. Given findings (58, 59) suggest that obesity associated cancer progression is due to immune suppression, we hypothesized that differences in ICI outcomes between DIO male and female mice were immune mediated. To better understand how the tumor microenvironment (TME) was impacting tumor kinetics we performed flow cytometry on 3LL tumors from lean and DIO mice of both sexes (Supplemental Figure 8A). Tumors in DIO mice had significantly decreased TME immune infiltrate assessed by CD45+ cells when compared to lean counterparts regardless of sex (Supplemental Figure 8B). In all groups CD11b+ myeloid cells were the predominant immune populations of 3LL tumors (Supplemental Figure 8C-D) as previously published (60), including tumor associated macrophages (TAMs) (CD11b+/F480Hi) (Figure 3A, Supplemental Figure 9A), and myeloid derived suppressor cells (MDSCs) (CD11b+/GR-1+) (Supplemental Figure 9B-C). Furthermore, the tumor immune infiltrate between lean and DIO mice differed with lean mice of both sexes having significantly higher levels of lymphocytes (including T,

Treg, NK, and NKT) and dendritic cells over DIO counterparts, while no difference was observed in B cell infiltrate (Supplemental Figure 9D-I).

Although TAMs were the most abundant immune cell type in all groups, DIO female mice had significantly higher percentages of TAMs than DIO males (Figure 3A). TAMs have been implicated as a negative prognostic indicator in clinical cancer outcomes (61), and reports indicate that TAMs are responsible for driving increased tumor growth in obesity (62). Additionally, estrogen signaling promotes M2 polarization (63), potentially contributing to immunotherapy resistance. To interrogate the role of TAMs in the obese TME across sex we evaluated the expression of MHC-II and CD206 on TAMs, both markers of interest for characterization of macrophage polarization (64, 65). Utilizing established nomenclature (63), M1 macrophages identified as MHC-II+ and CD206- and M2 macrophages as MHC-II- and CD206+, we evaluated the ratio of M2/M1 macrophages (Figure 3B-C). We observed that lean male mice showed the lowest M2/M1 ratio, driven in part by increased M1 TAMs, DIO male and lean female mice had comparable ratios, while DIO females had the highest M2/M1 ratio and were significantly higher than that observed in DIO male mice (Figure 3B). Further analysis identified that DIO female mice had significantly lower expression of MHC-II on TAMs than DIO males both by MFI (Figure 3D-E) and by total percentage on TAMs (Supplemental Figure 9J). Importantly, after anti-PD-1 therapy tumor infiltrating T cells increased significantly only in DIO males (Figure 3F).

To further characterize the TME of both male and female DIO mice, we performed bulk RNAseq analysis of 3LL tumors. Principal component analysis (PCA) demonstrated clustering based upon diet and biologic sex with the latter being most pronounced (Supplemental Figure 10A). Tumors from lean male and female mice had significant differences in expression of 344 genes (Supplemental Figure 10B), while 2009 genes were significantly different between male and female DIO mice (Figure 3G). Of these differentially expressed genes between DIO male and female mice only 213 were also differentially expressed between lean male and female mice leaving 1796 genes differentially expressed by sex only in obese mice (Supplemental Figure 10C). Further analysis revealed

significant upregulation of *Cd68* expression (Supplemental Figure 10D), a marker of TAMs, in DIO female mice. Additionally, *Trem2,* a marker of lipid associated macrophages, was also significantly elevated in DIO female mice when compared to DIO males (Supplemental Figure 10E). Several genes including *Il1ra*, *Nos2*, and *Cxcl9* associated with M1 polarization were significantly upregulated in DIO male mice (Figure 3H). Conversely, an array of genes associated with M2 polarization *Msr1, Fuca2, Dhrs3, Folr2, Irf4, and P2ry1* were significantly upregulated in DIO females (Figure 3I).

To evaluate translation to human tumors we investigated sequencing data from Caris Life Sciences. Using immune deconvolution, we assessed differences in M2 macrophages and T cells from tumors of melanoma and NSCLC patients. High BMI male melanoma patients demonstrated increased T cells and decreased M2 polarization compared to high BMI females (Supplemental Figure 10F), while male NSCLC patients also had decreased M2 polarization when compared to high BMI females (Supplemental Figure 10G).

Metabolomic profiling reveals links across species in obesity and identifies distinctions based on sex. Recent evidence has demonstrated that metabolic profiles can offer insight into characterizing obesity and may have an influential role on tumor growth, immunotherapy, and may differ based upon sex (66). To establish a relevant metabolomic signature, we evaluated serum from normal BMI (BMI < 25) and obese (BMI > 30) human patients in an exploratory study. These patients treated with immunotherapy presented with stable, progressive, or hyper-progressive disease. Samples were subjected to metabolomics assessment and the top twenty-six differentially abundant metabolites in normal and obese patients were identified (Figure 4A, Supplemental Figure 11A).

Serum from the DIO mouse model was also assessed evaluating metabolomic differences through several comparisons across diet, sex, or combination of the two factors. Comparisons included lean male vs DIO male, lean female vs DIO female, lean male vs lean female, and DIO male vs DIO female (Figure 4B-E, Supplemental Figure 11B). Starting with diet, DIO male mice had 176 differentially abundant metabolites when compared to their lean male counter parts (Figure 4B), while

DIO females only had 43 significantly different metabolites from their lean counterparts (Figure 4C). Lean male and female mice had 105 differentially abundant metabolites, yet when looking at the metabolite differential between DIO male and female mice, there were far greater differences than related to diet or sex alone with 321 significantly different metabolites of which 94 were uniquely differential (Figure 4D-E).

Using the metabolite signature from the human samples, we evaluated the metabolite quantitation for the identified metabolites in DIO mice. We observed that DIO male mice had higher levels of all six metabolites that were elevated in obese human patients (Figure 4F). DIO female mice only had increased levels in four metabolites over DIO males all of which were decreased in the human obesity signature (Figure 4G). DIO male mice also had elevated levels of ten metabolites decreased in the human samples (Supplemental Figure 11C), while the remaining metabolites in the human signature had no significant difference between DIO male and female samples (Supplemental Figure 11D). These data illustrate that metabolomic signatures may provide insight into a diverse spectrum of obesity.

Prior-ovariectomy restores the immunotherapy response in DIO female mice and mediates changes in hormonal profile. Sex hormones, including androgens (48, 50) and estrogens (51, 63), can negatively impact efficacy of ICI response. We next aimed to interrogate whether estrogen signaling was acting as a deterrent for ICI success in DIO female mice. To address this, we ovariectomized female mice prior to initiating a HFD diet, monitored weight gain after diet commenced, and then assessed the impact of ovariectomy on DIO phenotype, tumor growth, and ICI responses (Figure 5A). Following ovariectomy, female mice placed on a HFD demonstrated similar weight kinetics as male counterparts on a HFD and gained weight faster than sham-ovariectomized female DIO mice, however by 16 weeks all mice on a HFD reached comparable weights (Supplemental Figure 12A-D). We then evaluated the tumor kinetics and *in vivo* efficacy of anti-PD-1 checkpoint blockade in these ovariectomized cohorts using B16F0 and 3LL syngeneic tumors. DIO male mice again demonstrated significantly reduced tumor burden following anti-PD-1 treatment in

both tumor models, while DIO female mice demonstrated no significant reduction in tumor growth. Strikingly, ICI treated DIO ovariectomized female (OVX) mice demonstrated significantly reduced tumor growth in B16F0 and 3LL challenged mice (Figure 5B-C, Supplemental Figure 12E). DIO male and OVX mice displayed significant reductions in tumor burden in the majority of anti-PD-1 treated mice in both tumor models while DIO female mice did not (Figure 5D-E). DIO OVX female mice treated with anti-PD-1 also experienced a significant improvement in survival (Supplemental Figure 12F). Flow cytometry analysis of TAMs from 3LL tumors again revealed that DIO male mice had significantly elevated levels of MHC-II and a decreased ratio of M2/M1 macrophages (MHCII- CD206+/MHCII+ CD206-) when compared to DIO female mice (Figure 5F-H). Notably, DIO OVX females demonstrated significantly higher MHC-II expression on TAMs, significantly lower M2/M1 macrophage ratios, and higher total CD45+ tumor infiltrate than DIO Female mice (Figure 5G-H, Supplemental Figure 12G). Following ICI, DIO female mice did not demonstrate increases in T cells while both DIO males and DIO OVX experienced significant increases in CD8 and CD4 T cells (Figure 5I-J). These data indicate that surgical ovariectomy augments responses to ICI in DIO female mice modulating macrophage polarization state, increasing T cell infiltrate, and promoting anti-tumor effects.

To better understand systemic hormonal levels in our model, we performed serum steroid analysis which revealed that DIO male mice had significantly more testosterone than DIO females (Supplemental Figure 12H). Assessment of estrogen levels revealed a significant reduction but not ablation of the estradiol in ovariectomized DIO female mice when compared to sham surgery DIO females (Supplemental Figure 12I). Ovariectomized female mice also demonstrated lower levels of 20a-dihydroprogesterone (Supplemental Figure 12J). The ratio between testosterones and estrogens were similar in DIO male and DIO ovariectomized female mice (a ratio of roughly 9:1,estradiol: testosterone) suggesting a connection to therapeutic response.

Stratification of female patients by age and BMI reveals distinctions in immunotherapy outcomes. To interrogate the implications of our pre-clinical data we reanalyzed our previously

assessed patient cohort focusing on female patients stratifying on BMI and age, as a surrogate readout for post-menopausal status. We hypothesized that post-menopausal (age ≥55) obese patients would have improved outcomes. Age played an important role, obesity was associated with improved OS with high BMI (BMI ≥ 30) female patients (age ≥55) demonstrating significant improvement in OS over female patients with BMI < 30 ($p = 0.003$, Figure 6A, Supplemental Table 4). Yet, obesity was seemingly not beneficial to female patients under 55, notably female patients (age < 55 and BMI < 30) trended toward better OS ($p = 0.0722$, Figure 6A, Supplemental Table 4). Assessing lung cancer patients from TCGA, we stratified female patients by the same parameters from the survival analysis (menopausal status, age < 55, or age ≥ 55) and compared to male patients. Using immune deconvolution (CIBERSORT), we assessed a signature of M2 macrophages across male, pre-menopausal female, and post-menopausal female lung cancer patients. Although BMI was not an included characteristic in the dataset, we did observe significant increases in M2 macrophage cell composition in pre-menopausal (age < 55) female patients when compared to both male and post-menopausal female (age ≥ 55) (Figure 6B). These findings illustrate that sex, and consequently hormonal levels may modulate immune responses particularly in the context of cancer and ICI.

Metabolomic signatures linking DIO male and ovariectomized females are associated with immunotherapy responses in vivo. Distinctions in the metabolomic profile between male and female mice, as well as lean and DIO phenotypes, prompted the identification of metabolomic components that may be distinct based on hormone signaling and predictive of immunotherapy. We performed metabolomic analysis on the serum of male, female, and OVX cohorts of mice (both lean and DIO). Principal component analysis demonstrated distinct clusters for each of the groups with DIO male samples being most distinguished from other groups (Figure 7A). An increased abundance of triacylglycerides (TG) and phosphatidylcholines (PC) were the most notable distinctions based on diet alone with DIO male, female and OVX mice having elevated TGs (Figure 7B). All DIO groups had significant metabolomic differences from their respective lean counterparts including DIO ovariectomized mice which demonstrated both increases and decreases in metabolites (Figure 7C).

Metabolomic profiles of DIO OVX mice were distinct from lean controls (Figure 7D), DIO males (Figure 7E) and DIO females (Figure 7F). Overall, DIO males demonstrated the greatest number of increased metabolites with 144 metabolites increased with obesity, while female and ovariectomized females had increases of 16 and 29 metabolites respectively (Figure 7C). DIO female mice had more deceased metabolites in obesity with 27 metabolites that were more abundant in lean counterparts (Figure 7C). Twenty Metabolites were found to be in common between DIO males and DIO OVX including lipids (TG(18:0_36:2), TG(20:4_36:4), TG(18:2_38:5), TG(18:2_38:6), TG(20:4_36:3), TG(18:3_38:6), TG(20:4_36:5), TG(20:4_34:2), TG(16:0_38:5), TG(20:4_34:1)), phosphatidylchlolines (PC aa C36:2, PC aa C38:4, PC aa C40:6) and ceramides/sphingolipids (Cer(d18:1/20:0), SM C22:3, SM C18:0, SM C18:1, SM (OH) C16:1, SM C16:0, Cer(d18:1/18:0)). PC aa C38:4 and PC aa C36:2 were correlated with decreases in tumor burden following anti-PD-1 across all DIO mice (Figure 7H-I). Conversely, alpha amino butyric acid (AABA), a metabolite associated with inhibiting M1 polarization (67) and significantly increased in DIO females, was found to be negatively associated with decreases in tumor burden following immunotherapy (Figure 7J).

To assess the connection of mouse and human metabolomic profiles, we performed pathway analysis comparing males (obese vs lean), pre-menopausal females (obese vs lean), and post-menopausal females (obese vs lean) which revealed similarities across groups in processes including nitrogen metabolism, biosynthesis of fatty acids, and alpha linoleic acid (Supplemental Figure 13A). We identified similarities between obese post-menopausal females and males most notably in glutathione metabolism as well as in phenylalanine and tyrosine metabolism, transulfuration, and arginine biosynthesis. We observed similar pathways between obese pre-menopausal females and male in nicotinamide adenine metabolism, arginine biosynthesis, prostanoid biosynthesis, glycerophospholipid metabolism, and folate metabolism (Supplemental Figure 13A). Profiling the metabolome may provide deeper insight into obesity and explain heterogeneity in the obese immune response. Notably, AABA a metabolite linked to inhibition of M1 polarization was increased in DIO females and overall associated with poorer tumor control in treated mice.

Discussion

Obesity is a complex condition that influences numerous biological processes including metabolism, immunology, and endocrinology, which contributes to a diverse spectrum of obese phenotypes. A growing body of literature is dedicated to understanding how obesity impacts patients, particularly in the context of cancer, and cancer immunotherapy. The association of obesity with improved outcomes to immunotherapy, notably ICIs, has been an important observation. Data implicating a sex-based association with ICI response has been reported, yet there remain questions as to what mechanisms are mediating this association and whether confounding variables including diet, metabolomic profiles, hormonal levels, and how obesity is defined (e.g. BMI) are impacting observations. This study investigates if obesity differentially impacts the efficacy of ICIs depending on biologic sex and explores the mechanisms driving therapeutic differences.

We report that from a cohort of 114 male patients treated with anti-PD-1/L1 ICIs those with a BMI ≥30 demonstrated improved OS and PFS when compared to male patients with a BMI < 30. In contrast, the corresponding cohort of 136 female patients treated with ICIs, didn't observe significant improvement in OS or PFS for female patients with BMI ≥ 30. We corroborated this observation in two larger patient cohorts of melanoma (1,185 male & 1,816 female) and NSCLC-adenocarcinoma (4,983 male & 4,278 female). Using a preclinical DIO model, we demonstrate tumors grew faster in both male and female DIO mice. When treated with anti-PD-1 in vivo, only DIO male mice had a significant reduction in tumor burden. When we examined the TME at baseline we found that DIO mice demonstrated reduced overall immune infiltrate, yet of this infiltrate DIO female mice had significantly more TAMs than DIO males. Additionally, not only were TAMs significantly increased in the tumors of DIO female mice, but the ratio of M2/M1 TAMs was significantly greater and accompanied by elevation of M2 associated genes. Performing ovariectomy on female mice prior to diet initiation improved therapeutic outcome to ICI and augmented the TME, decreasing the ratio of M2/M1 TAMs and promoting increases in tumor infiltrating T cells. We stratified obese female patients by age, as a

surrogate for menopausal status, and identified that obese women 55 years of age and older had better outcomes than obese women younger than 55. Further, TCGA analysis of lung cancer patients revealed that women above age 55 had a M2 signature significantly lower than women below age 55, the former being comparable to male patients. Lastly, we investigated distinctions in metabolomic profile across male and female mice. We observe that DIO male mice demonstrate greater differences in metabolites than DIO females and that specific metabolites are modulated through ovariectomy and are associated with ICI efficacy.

We identify that obesity status is associated with better outcomes for male but not female cancer patients undergoing ICIs and our preclinical studies suggest this is driven mechanistically by TAMs shifted toward M2 like phenotypes through hormonal and metabolic signaling leading to immune suppression and decreased efficacy of ICIs. The observation that obesity can influence the cancer immune landscape is not new. Studies from Wang et al (2019) (24), illustrated that obesity positively augments the obese tumor environment in the context of ICI. Subsequent reports from Ringel et al (2020) (58) further implicated the role of immunity in tumor control within the obese environment identifying that tumor cells and tumor infiltrating $CD8^+$ T cells differentially adapt to the obese environment. Dyck et al (2022) (68) also focused on $CD8^+$ T cells and illustrates that immunotherapy can improve $CD8^+$ T cells functionality in the obese environment. Although T cells are the primary targets of ICIs and the predominate mediators of anti-tumor killing our data suggest that the net outcome from ICI is dependent on more than a single cell type. We identify TAMs as another key influencer within the obese TME. Recent publications from Bagchi et al (2024) (62) and Bader et al (2024) (59) support these data both implicating TAMs as major contributors to the suppressed immune response in the obese TME. The current study demonstrates that TAMs are increased in the tumors of DIO female mice, have greater M2 polarization, and that ovariectomy can augment TAM polarization. Our observations suggest that hormonal signaling influences TAM polarization in obesity and this aligns with the findings of Chakraborty et al (2021) (63) which identify that estrogen signaling can elicit a shift toward M2 macrophage polarization ultimately decreasing ICI success. AABA, a

metabolite previously identified as constraining inflammatory (M1) macrophage polarization[68], is elevated in DIO female mice and negatively correlated with reduction in tumor burden following anti-PD-1.

Although data link estrogen to M2 polarization and immune suppression, other studies from Dupuychaffray et al (2025) (51) suggest adipocyte derived estrogens are beneficial in obese male patients treated with ICI. They identify that in males estrogens promote antigen presentation by dendritic cells and increase $CD8^+$ T cell cytotoxicity (51). However, estrogens do not work in isolation, androgens, elevated in males, also can suppress ICI responses. Kwon et al (2022) (50) and Guan et al (2022) (48) identified that androgen signaling impairs T cell immunity. With both androgens and estrogens influencing an immune response, the levels of these hormones and their respective ratios become important. In the context of ICI, understanding the direct effects of estrogens and androgens on T cells and the influence on TAMs offers an explanation as to why obese males, characterized by increased estrogens and decreased androgens, demonstrate improved responses.

Despite current findings, there remains controversy on whether there is a true association between obesity and improved ICI outcomes clinically. Thus, it becomes important to acknowledge present limitations in interrogation of these questions. A major limitation resides in defining obesity. This study relied on the use of BMI, yet BMI alone is an imprecise metric that can falsely categorize those with high muscle mass as obese and may not capture individuals with high adiposity and sarcopenia (69–71). Importantly, there are inherent differences in adiposity and adipose tissue distribution between male and females with the latter generally having greater adiposity and increased subcutaneous adipose tissue (SAT), while males are disposed to more abdominal adipose tissue or visceral adipose tissue (VAT) (72, 73). Alternative methodologies to define obesity, such as measuring fat content (74–76) and sarcopenia on MRI or CT scans, hip-to-waist ratios, or inflammatory indices, have also demonstrated associations with ICI efficacy (74, 77–80). Metabolomic considerations should also be taken into account when defining obesity as recent data has suggested specific fatty acids can have direct influence on cancer cells and immunity (62, 81). Though we identify a metabolomic signature

for obesity and correlate metabolites with response to ICI this was exploratory. Access to human hormonal or metabolomic data matched to OS and PFS was not attainable. Identification of ideal human metabolite and hormonal profiles will be paramount, and it will be important to characterize the heterogeneity in human obesity and the connection to BMI, adiposity, or diet.

There remain substantive limitations in modeling obesity preclinically. Particularly, given that standardized murine diets (e.g. LFD or HFD) do not recapitulate the diverse array of human diets there are limitations on translation 1:1. It will be important to evaluate the contributions of both adiposity and diet to the metabolomic profile particularly in the context of recent data from Kunkemoeller et al (2025) (82) which suggests that the source of dietary fat can have a marked impact on immunity and metabolism and Desharnais et al (2026) (83) which indicate diet directly influences response to ICI. Here in this study the individual contributions of diet and adiposity were not delineated and related factors including host microbiome require further exploration. Beyond diet considerations, there is a substantial gap between preclinical DIO models and the clinic. Hahn et al (2023) (84) report an example of this, where tumors from high BMI melanoma patients were observed to have no difference in tumor mutational burden when compared to patients with low BMI, and surprisingly were also found to be more metabolically quiescent than those from low BMI patients. This opposes observations in preclinical DIO murine models in which tumors grow faster and are not quiescent. Hahn et al (2023) (84) also did not observe significant differences in their assessments of tumors based on patient sex. An intrinsic limitation of murine models is their age. Even after months on a DIO regimen mice used in preclinical studies are young relative to human cancer patients. In the present study this limitation can be a complicating variable as menopause is not experienced in mice outside of interventions such as ovariectomy.

Future preclinical and clinical studies should assess variables including the role of adiposity, adipose distribution, diet, metabolic parameters, inflammatory scores, sarcopenia or muscle mass, and even hormonal levels as BMI or body weight differential fails to capture these relevant parameters. Dissection of obese parameters that are favorable to ICI and drive anti-tumor effects still need to be

evaluated. In assessment of the role of patient sex, additional studies are needed to assess the direct effects of hormonal signaling in obesity and evaluate whether hormonal therapy with agents targeting estrogen (e.g. tamoxifen, anastrozole, fulvestrant), or androgen receptor (AR) (e.g. enzalutamide, apalutamide, and darolutamide) may modulate immune responses to therapy and impact cancer progression. Outside of obesity Chakraborty et al (2021) (63) has already demonstrated that therapeutic treatment using fulvestrant improves ICI responses and AR antagonists are already being investigated in immune responsive cancers such as melanoma (85). Further interrogation of hormonal inhibitors with ICIs in a clinical setting will be informative. Given contrasting effects in a DIO model delineated based upon biologic sex, it suggests that it is insufficient to rely on DIO models of a single sex as this may fail to capture the full spectrum of obesity. Metabolomic considerations may better categorize obesity states and identify conditions that are most receptive to a given treatment. Preclinical studies can address these questions by interrogating hormone interactions in obesity and offer translational opportunities by providing potential biomarkers such as hormonal levels and their respective ratios. Clinical studies should assess metabolomic and hormonal readouts and evaluate their impact on therapeutic efficacy and toxicities. These approaches may provide insights into therapeutic responses or pipelines for patient care.

With a growing overweight and obese population, and an increasing prevalence of obesity-associated cancers, it is important to consider the diverse clinical manifestations of obesity and how these impact a patient's response to therapy. The current study concludes that biologic sex and consequently hormonal and metabolic pathways directly affect the obese TME through modulation of the immune landscape and impact the outcomes of ICIs.

Methods

Sex as a biologic variable: Human data relied upon male and female patients and the impact of sex as a biologic variable was a foundation of studies. All animal models incorporated male and female mice for all experiments presented.

Animal Models: Male and female C57BL/6 mice were obtained at 6-8 weeks in age from Taconic farms and housed under specific pathogen free conditions within animal facilities at the University of California Davis. DIO and age matched control mice were generated through feeding of diets containing 60% or 10% fat for at least four months (Research Diets D12492 & D12450J). Animals receiving ovariectomies were purchased from Taconic Farms post-surgery and were monitored daily during recovery until surgical clips were removed. Mice were monitored weekly with bi-weekly assessment of weight kinetics. Animals used in tumor studies were randomly assigned into treatment groups while ensuring comparable tumor burdens between untreated and treatment prior to administering a loading dose. In vivo mouse studies were done at least twice to ensure reproducibility of results.

Cell Culture, Tumor cell lines and models: C57BL/6 syngeneic murine cell lines B16F0 melanoma (CRL -6322) and Lewis lung carcinoma (3LL, CRL -1642) were obtained from ATCC. Cells were cultured in complete RF10c media containing 10% Nu Serum (Corning, IV Culture, catalog 355504), 2 mM glutamine (Gibco, catalog 25030-081), 1% nonessential amino acids (Corning, catalog 25-025-CI), 1% penicillin-streptomycin (Corning, catalog 30-002-CI), 5 × 10–5 M 2-mercaptoethanol (Sigma-Aldrich, catalog M7522-100), 1 M HEPES buffer (Gibco, catalog 15630-080), and 1 mM sodium pyruvate (Corning, catalog 25-000-CI) at 37°C, 5% CO2. Tumors were implanted into C57BL/6 mice through subcutaneous injection of $1x10^6$ B16F0 or 3LL cells suspended in 100µl PBS into the right flank. Mice were monitored daily with routine tumor measurements taken every 2-3 days once tumors were palpable. Tumor volume was calculated by length (mm) x width $(mm)^2$ x 0.5. Measurements were conducted by one measure through the course of the study using electronic calipers and measurements were performed independent of group assignment though.no explicit blinding was performed. In experiments including anti-PD-1 immune checkpoint therapy treated mice received a loading dose of 500ug of either anti-PD-1(Clone 29 F.1A12, BioXCell) or rIgG (Jackson ImmunoResearch, Inc) through intraperitoneal injection followed by subsequent doses of 250µg every other day for a maximum of six doses.

Flow Cytometry: Flow Cytometry staining was performed on single cell suspension of lymph node, spleen, tumor, and peripheral blood. Solid tissues were harvested and mechanically homogenized and filtered in preparation for staining. For processing of tumor enzymatic digestion was performed and utilized a mouse tumor dissociation kit from Miltenyi Biotec (CAT: 130-096-730). Cells were stained for viability using Zombie Red (BioLegend), Zombie NIR (BioLegend) or Fixable Viability Dye 780 (Invitrogen). Fc blocking was performed by incubating cells with Fc Block (anti-CD16/32 clone 93) for 10-15 minutes followed by a surface stain of fluorochrome-conjugated monoclonal antibodies in staining buffer (phosphate-buffered saline + 3% Nu serum) for 30 minutes. For stains involving intracellular markers, cells were permeabilized using Cytofix/Cytoperm (BD Biosciences) for 20 min and washed prior to use of intracellular antibodies or with a FOXP3/transcription factor fixation/permeabilization kit (eBiosciences) according to the manufacturer's specification. Antibodies(Biolegedn&Invitrogen): PB-anti-CD45 (30-F11) (103126), PB-anti-CD44 (IM7)(103002), APC-Cy7-anti-CD45 (30-F11) (103116), BV711-anti-CD4 (RM4–5) (100550), BV785-anti-CD3 (17A2)(100232), BV605-anti-CD8a (53–6.7)(100744), Alexa Fluor 700-anti-Ki67 (16A8)(652420), FITC/PE-anti-PD-1 (RMP1–30) (50-101-05/109104), PE-anti-Tim3 (RMT3–23)(25-5870-82), PerCP-eFluor 710-anti-Lag3 (eBioC9B7W)(46-2231-82), and PE-Cy7-anti-CD62L (MEL-14)(104418). Spectral flow cytometry was performed on a Sony ID7000 and FluoroFinder was utilized for panel design and construction (Supplemental Table 5).

Metabolomics: Murine serum was obtained through centrifugation of blood samples in BD microtainer tubes (BD Biosciences, 365967). Blood was obtained either through tail vein or at humane endpoint cardiac puncture. Serum samples were shipped and analyzed at Roswell Park Comprehensive Cancer Center Bioanalytics, Metabolomics, and Pharmacokinetics Shared Resource, using the MxP Quant 500 kit (Biocrates Life Sciences AG, Innsbruck, Austria) in accordance with the user manual. 10 µL of each supernatant, quality control (QC) samples, blank, zero sample, or calibration standard were added on the filter spot (already containing internal standard) in the appropriate wells of the 96-well plate. The plate was then dried under a gentle stream of nitrogen. The

samples were derivatized with phenyl isothiocyanate (PITC) for the amino acids and biogenic amines and dried again. Sample extract elution was performed with 5 mM ammonium acetate in methanol. Sample extracts were diluted with either water for the HPLC-MS/MS analysis (1:1) or kit running solvent (Biocrates Life Sciences AG) for flow injection analysis (FIA)-MS/MS (50:1), using a Sciex 5500 mass spectrometer. Data were processed using MetIDQ software (Biocrates Life Sciences AG, vsn Oxygen-DB110-3005), and Limma (vsn 3.56.2) for differential metabolite analysis. Human serum samples were obtained through biorepository at Roswell Park Comprehensive cancer and metabolomics analysis was performed as described above. Patient samples ranged in age from 47-79 years in age with 7/8 samples being male; samples were deidentified and all data was handled through an honest broker.

RNA Extraction, PCR, sequencing, and analysis: Total RNA was extracted from whole tumor tissue stored in RNAlater using RNeasy plus mini kit (Qiagen). Tumor samples were placed in RNAlater immediately after tissue collection and allowed to rest at 4 degrees for at least 24 hours. RNA concentrations were quantified using a Qubit fluorometer and RNA integrity was assessed using TapeStation 2200 (Agilent). mRNA was submitted either to the UC Davis Genomics core or to Novogene for strand-specific library preparation and sequenced on a HiSeq 2500 instrument (150 pair-end sequencing). Data analysis was performed by the UC Davis Bioinformatics core using expHTS to trim low-quality sequences and adapter contamination and to remove PCR duplicates from raw reads.

Human PD-(L)1 clinical data: Clinical data was obtained as previously described (24) from an IRB-approved at the University of Oklahoma Health Sciences Center from patients treated with anti PD-1 and PD-L1 therapy between January 2014 and January 2018 ($n = 250$). Data was stratified based off sex and as previously performed a Kaplan–Meier analysis was used to assess BMI category (<30 versus ≥30) and its relation to survival (OS) and progression-free survival (PFS).

Caris Body Mass Index Classification: Patients with melanoma (n=3,004) and non-small cell lung cancer (NSCLC) (n=16,523) who received immune checkpoint inhibitor (ICI) therapy and had a body mass index (BMI) measurement closest to the initiation of ICI treatment were included in this analysis. Obesity was defined as a BMI ≥30 according to the World Health Organization (WHO) classification, while patients with BMI <30 were classified as non-obese. Patients were further stratified by sex, resulting in four study groups: non-obese male, obese male, non-obese female, and obese female.

Caris Survival Analysis: Overall survival (OS) was defined as the interval from initiation of immune checkpoint inhibitor (ICI) therapy to death from any cause or the date of last clinical follow-up. Patients who were alive at the time of last follow-up were censored. Kaplan–Meier survival curves were generated separately for male and female patients to compare obese (BMI ≥30) and non-obese (BMI <30) groups, and survival distributions were compared using the log-rank test. To evaluate whether the association between obesity and overall survival differed by sex, a Cox proportional hazards regression model including obesity, sex, and a sex-by-obesity interaction term (sex × obesity) was fitted. Obesity was treated as a binary variable (BMI ≥30 vs. BMI <30), and sex was treated as a binary variable (male vs. female). The statistical significance of the interaction term was used to assess whether the effect of obesity on overall survival differed between males and females. Hazard ratios (HRs), corresponding 95% confidence intervals (CIs), and two-sided P values were reported. A two-sided interaction P value <0.05 was considered statistically significant.

Data availability: Values for data presented in the manuscript can be found the “Supporting data values”. The bulk RNAseq data presented in the study are deposited in the NCBI BioProject repository, accession number PRJNA925221.

Immune Cell Infiltration Analysis: Tumor immune cell composition was estimated from whole-transcriptome sequencing (WTS) data using quanTIseq, a computational deconvolution algorithm that infers the relative fractions of immune cell populations from bulk RNA sequencing data. Estimated fractions of macrophage M1, macrophage M2, $CD4^+$ non-regulatory T cells, and $CD8^+$ T cells were

extracted for each tumor sample. Mean (median) immune cell fractions were calculated within each BMI/sex subgroup. The M2/M1 macrophage ratio was calculated as the ratio of the mean (median) estimated M2 macrophage fraction to the mean (median) estimated M1 macrophage fraction for each subgroup. Immune infiltration profiles were visualized using heatmaps and violin plots.

Magnetic resonance imaging: Mice used for imaging were anesthetized using a combination of isoflurane and oxygen prior to scanning on a Biospec 70/30 7.0-Tesla small-animal magnetic resonance imaging (MRI) system (Bruker Biospin Inc.) using a 60-mm quadrature transmitter/receiver coil for whole-body imaging. Scanning protocols and procedures were done as previously described (53, 86).

Leptin and Glucose measurements: Serum Glucose (Fisher Diagnostics Middletown, VA) and blood Hemogobin A1c (Diazyme Poway, CA) enzymatic assays were performed by UC Davis Mouse Metabolic Phenotyping Center (MMPC). Serum Leptin was measured using an electro-chemiluminescent assay (Meso Scale Discovery) and through leptin (mouse) ELISA from Enzo (ADI-900-019A). Confirmatory glucometer measurements used an Alphatrak meter in accordance with manufacturer parameters for mice.

Statistics: Graphs and statistical analyses were prepared using Prism software (GraphPad Software Inc., CA USA) and R. Data were expressed as mean ± s.e.m, unless otherwise noted. For analysis of three or more groups, one-way analysis of variance (ANOVA) was performed with a Bonferroni, Sidak, or Tukey *post-hoc* test, when appropriate. Repeated measures two-way ANOVA (or mixed analysis when applicable) were used in instances of repeated measurements. Analysis of differences between two normally distributed test groups was performed using the student's *t*-test (two-tailed). *P* values were considered statistically significant if $P < 0.05$. Statistical outliers were identified using Grubb's test. Statistical differences in survival were determined by log rank (Mantel–Cox) analysis. For human data collected by Caris Life Sciences: Continuous variables were compared using the Wilcoxon rank-sum (Mann–Whitney U) test. Kaplan–Meier survival curves were compared using the

log-rank test. Cox proportional hazards regression was used to estimate hazard ratios and 95% confidence intervals where applicable. All statistical analyses were performed using Python (version 3.x) with the pandas, NumPy, SciPy, lifelines, matplotlib, and seaborn packages. All statistical tests were two-sided, and a P value <0.05 was considered statistically significant.

Study Approval: All in vivo murine studies were conducted in accordance with the UC Davis IACUC guidelines under an approved protocol. Human data collection for retrospective survival analyses at the University of Oklahoma Health Sciences Center was all in accordance with an IRB-approved protocol and de-identified.

Manuscript information

Author Contributions: LVV wrote the main manuscript. WJM and AMM supervised the project. LVV, AMM and WJM designed experiments. LVV, SRR, AMM, AMR all performed murine data analysis and interpretation. LVV, CC, LTK, MS, WAF, YHS, and RN performed murine experiments and data collection. SRR, YY, HB, ESA, AE, NG, RA, SI, MM, SKV and SM performed human data analysis and interpretation. LVV, SRR, YY, and MM assisted in figure preparation. LVV composed figures. SRR, RJC, SM, SG, LTK, SJJ, and AMM contributed to the manuscript based on their relevant expertise and provided critical review. All authors reviewed the manuscript.

AI disclosure: The authors declare that no AI tools were used in the original research for or writing of this article.

Conflict of interests: SM has received research funding from Ipsen Biopharmaceuticals/North American Neuroendocrine Tumor Society, which was paid to the institute and is outside the scope of this work. SM received consulting fees from Merck, Eisai, BMS, Gilead, and BeiGene/BeOne Ltd. SG declares consulting/ advisory board fees from Puma biotechnology, EMD Serono, Eisai Inc., Aveo. Research funding (paid to the institution) from AstraZeneca, Janux Therapeutics, Adicet Therapeutics, Inc., Xencor, Inc., ONCOC4, Inc. HB is a consultant/advisory board for BMS, Lilly, Genentech, Pfizer, Merck, EMD-Serono, Boehringer Ingelheim, Astra Zeneca, Novartis, Genmab, Regeneron, BioNTech,

Amgen, Axiom, PharmaMar, Takeda, Mirati, Daiichi, Guardant, Natera, Oncocyte, Beigene, iTEO, Jazz, Janssen, Puma, BerGenBio, Bayer, Iobiotech, Grid Therapeutics, RAPT, Gilead, Abbvie, Novocure, Summit, Astellas, Systimmune, University of Pennsylvania: CAR T Program, Takeda, Incyte, Novartis, Springworks, Servier, Sonnetbio; Inspirna; Nucleai, & ORIC. HB receives research support from BMS, Lilly, & Amgen.

Funding support: This work is the result of NIH funding, in whole or in part, and is subject to the NIH Public Access Policy. Through acceptance of this federal funding, the NIH has been given a right to make the work publicly available in PubMed Central. AMM and LVV were supported by NIH grant 1R01CA240751-01A1 and 3R01CA240751-01A1S1. This project was supported by the UC Davis Flow Cytometry Shared Resource Laboratory with funding from NCI P30 CA093373, S10 OD0034245 and S10 RR026825. UC Davis MMPC was supported by NIH/NIDDK Grant #U2CDK135074. Support by National Cancer Institute (NCI) grant P30CA016056 from Roswell Park Comprehensive Cancer Center's Bioanalytics, Metabolomics, and Pharmacokinetics Shared Resource. SJJ is supported by the UC Davis Paul Calabresi Career Development Award for Clinical Oncology funded by NCI/NIH grant #5K12-CA138464.

Acknowledgements: Figures were created with assistance from BioRender.com (https://BioRender.com/s8l8idy, https://BioRender.com/6wrf4uv, https://BioRender.com/665y9v7, https://BioRender.com/nf35tqy). Flow cytometry technical assistance and support was provided by Jonathan Van Dyke.

Address for correspondence: Department of Dermatology and Department of Internal Medicine, University of California Davis School of Medicine, Sacramento, CA 95817, USA. Email: wmjmurphy@ucdavis.edu Telephone: (1) 916-703-9397 Fax: (1) 916-703-5068, Postal Address: Institute for Regenerative Cures (IRC) 2921 Stockton Blvd, Suite 1630, Sacramento CA, 95817, USA.

References

1. Bagchi S, Yuan R, Engleman EG. Immune Checkpoint Inhibitors for the Treatment of Cancer: Clinical Impact and Mechanisms of Response and Resistance. *Annual Review of Pathology: Mechanisms of Disease*. 2021;16(Volume 16, 2021):223–249.

2. Doroshow DB, et al. PD-L1 as a biomarker of response to immune-checkpoint inhibitors. *Nat Rev Clin Oncol*. 2021;18(6):345–362.

3. Yarchoan M, et al. PD-L1 expression and tumor mutational burden are independent biomarkers in most cancers. *JCI Insight*;4(6):e126908.

4. Goodman AM, et al. Tumor Mutational Burden as an Independent Predictor of Response to Immunotherapy in Diverse Cancers. *Mol Cancer Ther*. 2017;16(11):2598–2608.

5. Holder AM, et al. Defining clinically useful biomarkers of immune checkpoint inhibitors in solid tumours. *Nat Rev Cancer*. 2024;24(7):498–512.

6. Landre T, Des Guetz G. Microsatellite instability-high status as a pan-cancer biomarker for immunotherapy efficacy. *Cancer Immunol Immunother*. 2025;74(4):122.

7. Vick LV, et al. Multifaceted effects of obesity on cancer immunotherapies: Bridging preclinical models and clinical data. *Seminars in Cancer Biology*. 2023;95:88–102.

8. Boutari C, Mantzoros CS. A 2022 update on the epidemiology of obesity and a call to action: as its twin COVID-19 pandemic appears to be receding, the obesity and dysmetabolism pandemic continues to rage on. *Metabolism*. 2022;133:155217.

9. Ogden CL, et al. Prevalence of Childhood and Adult Obesity in the United States, 2011-2012. *JAMA*. 2014;311(8):806–814.

10. Abarca-Gómez L, et al. Worldwide trends in body-mass index, underweight, overweight, and obesity from 1975 to 2016: a pooled analysis of 2416 population-based measurement studies in 128·9 million children, adolescents, and adults. *The Lancet*. 2017;390(10113):2627–2642.

11. Müller MJ, Geisler C. Defining obesity as a disease. *Eur J Clin Nutr*. 2017;71(11):1256–1258.

12. Jin Q, et al. Severe obesity, high inflammation, insulin resistance with risks of all-cause mortality and all-site cancers, and potential modification by healthy lifestyles. *Sci Rep*. 2025;15(1):1472.

13. Nevill AM, et al. Relationship between adiposity and body size reveals limitations of BMI. *American Journal of Physical Anthropology*. 2006;129(1):151–156.

14. Rothman KJ. BMI-related errors in the measurement of obesity. *Int J Obes*. 2008;32(3):S56–S59.

15. Shah NR, Braverman ER. Measuring Adiposity in Patients: The Utility of Body Mass Index (BMI), Percent Body Fat, and Leptin. *PLOS ONE*. 2012;7(4):e33308.

16. Sardinha LB, et al. A Comparison between BMI, Waist Circumference, and Waist-To-Height Ratio for Identifying Cardio-Metabolic Risk in Children and Adolescents. *PLOS ONE*. 2016;11(2):e0149351.

17. Pati S, et al. Obesity and Cancer: A Current Overview of Epidemiology, Pathogenesis, Outcomes, and Management. *Cancers*. 2023;15(2):485.

18. Kolb R, Sutterwala FS, Zhang W. Obesity and cancer: inflammation bridges the two. *Current Opinion in Pharmacology*. 2016;29:77–89.

19. Goodwin PJ, Stambolic V. Impact of the Obesity Epidemic on Cancer. *Annual Review of Medicine*. 2015;66(Volume 66, 2015):281–296.

20. Petrelli F, et al. Association of Obesity With Survival Outcomes in Patients With Cancer: A Systematic Review and Meta-analysis. *JAMA Network Open*. 2021;4(3):e213520.

21. Lysaght J, Conroy MJ. The multifactorial effect of obesity on the effectiveness and outcomes of cancer therapies. *Nat Rev Endocrinol*. 2024;20(12):701–714.

22. McQuade JL, et al. Association of body-mass index and outcomes in patients with metastatic melanoma treated with targeted therapy, immunotherapy, or chemotherapy: a retrospective, multicohort analysis. *The Lancet Oncology*. 2018;19(3):310–322.

23. Kichenadasse G, et al. Association Between Body Mass Index and Overall Survival With Immune Checkpoint Inhibitor Therapy for Advanced Non–Small Cell Lung Cancer. *JAMA Oncology*. 2020;6(4):512–518.

24. Wang Z, et al. Paradoxical effects of obesity on T cell function during tumor progression and PD-1 checkpoint blockade. *Nat Med*. 2019;25(1):141–151.

25. Caan BJ, et al. Explaining the Obesity Paradox: The Association between Body Composition and Colorectal Cancer Survival (C-SCANS Study). *Cancer Epidemiol Biomarkers Prev*. 2017;26(7):1008–1015.

26. Naik GS, et al. Complex inter-relationship of body mass index, gender and serum creatinine on survival: exploring the obesity paradox in melanoma patients treated with checkpoint inhibition. *j immunotherapy cancer*. 2019;7(1):89.

27. Richtig G, et al. Body mass index may predict the response to ipilimumab in metastatic melanoma: An observational multi-centre study. *PLOS ONE*. 2018;13(10):e0204729.

28. Sanchez A, et al. Transcriptomic signatures related to the obesity paradox in patients with clear cell renal cell carcinoma: a cohort study. *The Lancet Oncology*. 2020;21(2):283–293.

29. Lalani A-KA, et al. Assessment of Immune Checkpoint Inhibitors and Genomic Alterations by Body Mass Index in Advanced Renal Cell Carcinoma. *JAMA Oncology*. 2021;7(5):773–775.

30. Santoni M, et al. Clinico-Pathological Features Influencing the Prognostic Role of Body Mass Index in Patients With Advanced Renal Cell Carcinoma Treated by Immuno-Oncology Combinations (ARON-1). *Clinical Genitourinary Cancer*. 2023;21(5):e309-e319.e1.

706 31. Takemura K, et al. Impact of Body Mass Index on Survival Outcomes of Patients with Metastatic Renal Cell Carcinoma
707 in the Immuno-oncology Era: A Systematic Review and Meta-analysis. *European Urology Open Science*. 2022;39:62–71.

708 32. Cortellini A, et al. Baseline BMI and BMI variation during first line pembrolizumab in NSCLC patients with a PD-L1
709 expression ≥ 50%: a multicenter study with external validation. *J Immunother Cancer*. 2020;8(2):e001403.

710 33. Ichihara E, et al. The impact of body mass index on the efficacy of anti-PD-1/PD-L1 antibodies in patients with non-
711 small cell lung cancer. *Lung Cancer*. 2020;139:140–145.

712 34. Cortellini A, et al. A multicenter study of body mass index in cancer patients treated with anti-PD-1/PD-L1 immune
713 checkpoint inhibitors: when overweight becomes favorable. *Journal for ImmunoTherapy of Cancer*. 2019;7(1):57.

714 35. Yoo S-K, et al. Outcomes Among Patients With or Without Obesity and With Cancer Following Treatment With
715 Immune Checkpoint Blockade. *JAMA Network Open*. 2022;5(2):e220448.

716 36. Mastrolonardo EV, et al. Improved survival with elevated BMI following immune checkpoint inhibition across various
717 solid tumor cancer types. *Cancer*. 2025;131(6):e35799.

718 37. Alden SL, et al. Pan-tumor analysis to investigate the obesity paradox in immune checkpoint blockade. *J Immunother*
719 *Cancer*. 2025;13(1):e009734.

720 38. Roccuzzo G, et al. Obesity and immune-checkpoint inhibitors in advanced melanoma: A meta-analysis of survival
721 outcomes from clinical studies. *Seminars in Cancer Biology*. 2023;91:27–34.

722 39. Ihara Y, et al. Immunotherapy and Overall Survival Among Patients With Advanced Non–Small Cell Lung Cancer and
723 Obesity. *JAMA Network Open*. 2024;7(8):e2425363.

724 40. Antoun S, et al. Protective effect of obesity on survival in cancers treated with immunotherapy vanishes when
725 controlling for type of cancer, weight loss and reduced skeletal muscle. *European Journal of Cancer*. 2023;178:49–59.

726 41. Boi SK, et al. Obesity diminishes response to PD-1-based immunotherapies in renal cancer. *J Immunother Cancer*.
727 2020;8(2):e000725.

42. Rutkowski P, et al. Body mass index (BMI) and outcome of metastatic melanoma patients receiving targeted therapy and immunotherapy: a multicenter international retrospective study. *J Immunother Cancer*. 2020;8(2):e001117.

43. Trinkner P, et al. Survival and immunotoxicities in association with sex-specific body composition patterns of cancer patients undergoing immune-checkpoint inhibitor therapy – A systematic review and meta-analysis. *European Journal of Cancer*. 2023;184:151–171.

44. Zhang X, et al. Androgen Signaling Contributes to Sex Differences in Cancer by Inhibiting NF-κB Activation in T Cells and Suppressing Antitumor Immunity. *Cancer Research*. 2023;83(6):906–921.

45. Yuan B, et al. Estrogen receptor beta signaling in CD8+ T cells boosts T cell receptor activation and antitumor immunity through a phosphotyrosine switch. *J Immunother Cancer*. 2021;9(1):e001932.

46. Shuai C, et al. Estrogen Receptor Downregulates Expression of PD-1/PD-L1 and Infiltration of CD8+ T Cells by Inhibiting IL-17 Signaling Transduction in Breast Cancer. *Front Oncol*. 2020;10. https://doi.org/10.3389/fonc.2020.582863.

47. Oh MS, Anker JF, Chae YK. High gene expression of estrogen and progesterone receptors is associated with decreased t cell infiltration in patients with NSCLC. *Cancer Treatment and Research Communications*. 2021;27:100317.

48. Guan X, et al. Androgen receptor activity in T cells limits checkpoint blockade efficacy. *Nature*. 2022;606(7915):791–796.

49. Jiang G, et al. Androgen receptor affects the response to immune checkpoint therapy by suppressing PD-L1 in hepatocellular carcinoma. *Aging (Albany NY)*. 2020;12(12):11466–11484.

50. Kwon H, et al. Androgen conspires with the CD8+ T cell exhaustion program and contributes to sex bias in cancer. *Science Immunology*. 2022;7(73):eabq2630.

51. Dupuychaffray E, et al. Estrogens determine the efficacy of cancer immunotherapy in obese males with melanoma. *JCI Insight*. 2025;10(14). https://doi.org/10.1172/jci.insight.189758.

52. Farag KI, Makkouk A, Norian LA. Re-Evaluating the Effects of Obesity on Cancer Immunotherapy Outcomes in Renal Cancer: What Do We Really Know? *Front Immunol*. 2021;12. https://doi.org/10.3389/fimmu.2021.668494.

53. Vick LV, et al. Aging augments obesity-induced thymic involution and peripheral T cell exhaustion altering the "obesity paradox." *Front Immunol*. 2023;13:1012016.

54. Khuat LT, et al. Obesity induces gut microbiota alterations and augments acute graft-versus-host disease after allogeneic stem cell transplantation. *Science Translational Medicine*. 2020;12(571):eaay7713.

55. Khuat LT, et al. Increased efficacy of dual proinflammatory cytokine blockade on acute GVHD while maintaining GVT effects. *Blood*. 2021;138(24):2583–2588.

56. Salinero AE, Anderson BM, Zuloaga KL. Sex differences in the metabolic effects of diet-induced obesity vary by age of onset. *Int J Obes*. 2018;42(5):1088–1091.

57. Litwak SA, et al. Estradiol Prevents Fat Accumulation and Overcomes Leptin Resistance in Female High-Fat Diet Mice. *Endocrinology*. 2014;155(11):4447–4460.

58. Ringel AE, et al. Obesity Shapes Metabolism in the Tumor Microenvironment to Suppress Anti-Tumor Immunity. *Cell*. 2020;183(7):1848-1866.e26.

59. Bader JE, et al. Obesity induces PD-1 on macrophages to suppress anti-tumour immunity. *Nature*. 2024;630(8018):968–975.

60. Inoue H, et al. Comprehensive immunophenotyping reveals distinct tumor microenvironment alterations in anti-PD-1 sensitive and resistant syngeneic mouse model. *Sci Rep*. 2025;15(1):8311.

61. Pittet MJ, Michielin O, Migliorini D. Clinical relevance of tumour-associated macrophages. *Nat Rev Clin Oncol*. 2022;19(6):402–421.

62. Bagchi S, et al. The acid-sensing receptor GPR65 on tumor macrophages drives tumor growth in obesity. *Science Immunology*. 2024;9(100):eadg6453.

63. Chakraborty B, et al. Inhibition of estrogen signaling in myeloid cells increases tumor immunity in melanoma. *J Clin Invest*. 2021;131(23). https://doi.org/10.1172/JCI151347.

64. Yi R, et al. MHC-II Signature Correlates With Anti-Tumor Immunity and Predicts anti-PD-L1 Response of Bladder Cancer. *Front Cell Dev Biol*. 2022;10. https://doi.org/10.3389/fcell.2022.757137.

65. Najafi M, et al. Macrophage polarity in cancer: A review. *Journal of Cellular Biochemistry*. 2019;120(3):2756–2765.

66. Rosario SR, et al. Metabolic Dysregulation Explains the Diverse Impacts of Obesity in Males and Females with Gastrointestinal Cancers. *International Journal of Molecular Sciences*. 2023;24(13):10847.

67. Li F, et al. α-Aminobutyric Acid Constrains Macrophage-Associated Inflammatory Diseases through Metabolic Reprogramming and Epigenetic Modification. *International Journal of Molecular Sciences*. 2023;24(13):10444.

68. Dyck L, et al. Suppressive effects of the obese tumor microenvironment on CD8 T cell infiltration and effector function. *Journal of Experimental Medicine*. 2022;219(3).

69. Bilen MA, et al. Combined Effect of Sarcopenia and Systemic Inflammation on Survival in Patients with Advanced Stage Cancer Treated with Immunotherapy. *The Oncologist*. 2020;25(3):e528–e535.

70. Prado CM, et al. Sarcopenia and cachexia in the era of obesity: clinical and nutritional impact. *Proceedings of the Nutrition Society*. 2016;75(2):188–198.

71. Takenaka Y, et al. Predictive impact of sarcopenia in solid cancers treated with immune checkpoint inhibitors: a meta-analysis. *Journal of Cachexia, Sarcopenia and Muscle*. 2021;12(5):1122–1135.

72. Gavin KM, Bessesen DH. Sex Differences in Adipose Tissue Function. *Endocrinol Metab Clin North Am*. 2020;49(2):215–228.

73. White UA, Tchoukalova YD. Sex dimorphism and depot differences in adipose tissue function. *Biochimica et Biophysica Acta (BBA) - Molecular Basis of Disease*. 2014;1842(3):377–392.

74. Lou J, et al. Explanation of the obesity paradox of immunotherapy in cancer patients using CT-derived adipose composition parameters: A systematic review and meta-analysis. *International Immunopharmacology*. 2025;144:113699.

75. Li Y, et al. Prognostic value of body adipose tissue parameters in cancer patients treated with immune checkpoint inhibitors. *Front Immunol*. 2025;16. https://doi.org/10.3389/fimmu.2025.1557726.

76. Makrakis D, et al. Effect of body tissue composition on the outcome of patients with metastatic non-small cell lung cancer treated with PD-1/PD-L1 inhibitors. *PLOS ONE*. 2023;18(2):e0277708.

77. Zhou Y, et al. The Influence of Visceral Adiposity on Overall Survival: Exploring "Obesity Paradox" Among Hepatocellular Carcinoma Patients Who Receiving Immunotherapy. *Journal of Hepatocellular Carcinoma*. 2024;11:1193–1206.

78. Wang J, et al. Association of computed tomography-based body composition with survival in metastatic renal cancer patient received immunotherapy: a multicenter, retrospective study. *Eur Radiol*. 2023;33(5):3232–3242.

79. Popinat G, et al. Sub-cutaneous Fat Mass measured on multislice computed tomography of pretreatment PET/CT is a prognostic factor of stage IV non-small cell lung cancer treated by nivolumab. *OncoImmunology*. 2019;8(5):e1580128.

80. Lee JH, et al. Visceral adiposity and systemic inflammation in the obesity paradox in patients with unresectable or metastatic melanoma undergoing immune checkpoint inhibitor therapy: a retrospective cohort study. *J Immunother Cancer*. 2022;10(8):e005226.

81. Michelet X, et al. Metabolic reprogramming of natural killer cells in obesity limits antitumor responses. *Nat Immunol*. 2018;19(12):1330–1340.

82. Kunkemoeller B, et al. The source of dietary fat influences anti-tumour immunity in obese mice. *Nat Metab*. 2025;7(8):1630–1645.

83. Desharnais L, et al. Diet–microbiome synergy underlies obesity-associated immunotherapy efficacy. *Nature*. 2026;1–12.

84. Hahn AW, et al. Obesity Is Associated with Altered Tumor Metabolism in Metastatic Melanoma. *Clinical Cancer Research*. 2023;29(1):154–164.

85. Robert C, et al. Phase I Study of Androgen Deprivation Therapy in Combination with Anti–PD-1 in Melanoma Patients Pretreated with Anti–PD-1. *Clinical Cancer Research*. 2023;29(5):858–865.

86. Khuat LT, et al. Mechanisms by Which Obesity Promotes Acute Graft-Versus-Host Disease in Mice. *Frontiers in Immunology*. 2021;12. https://www.frontiersin.org/articles/10.3389/fimmu.2021.752484. Accessed July 26, 2022.

Figure 1. Obesity is associated with better outcomes in male, but not female patients receiving immune checkpoint inhibitors. (A-B) Kaplan-Meier estimates (product-limit survival estimates) with number of patients at risk of overall survival and progression free survival of 114 male and (C-D) 136 female patients receiving PD-1/L1 ICI stratified based on BMI < 30 (LT) or ≥ 30 (GTE) (n =114, 136).

Figure 2: **Male but not female DIO mice demonstrate decreased tumor burden and improved anti-tumor responses following anti-PD-1 immunotherapy.** (A) Weight (grams) of C57BL/6 mice over the course of diet regimen (n =19-20). Data representative of at least four cohorts/experiments. (B) Magnetic resonance images of lean and DIO male and female mice post diet regimen. (C) Schema detailing experimental design of lean and DIO mice implanted with subcutaneous tumors and treated with anti-PD-1 or isotype control until tumor assessment. (D-E) Tumor growth curves of untreated lean and DIO mice grouped by sex implanted subcutaneously with syngeneic tumor lines (D-E) B16F0 (n =4-6) a single experiment representative of 3 independent experiments and (F-G) 3LL (n = 11-12) data pooled from two experiments representative of 5 independent experiments. (H-I) Waterfall plots depicting change in tumor volume of anti-PD-1 treated mice from corresponding controls for male and female lean/DIO C57BL/6 mice implanted with (H)B16F0 & (I) 3LL (n = 5 - 12). Two-way ANOVA with multiple comparisons was used for analysis of (D-E and H-I), ns: not significant, $p \leq 0.05$.

Figure 3. Obesity differentially modulates the tumor microenvironment based on biologic sex promoting increased M2 tumor associated macrophages in DIO female mice. (A) Quantified percentages of CD11b+F4/80Hi cells of live CD45+ cells in 3LL tumors from lean and DIO mice of both sexes, pooled from three experiments (n = 11-17). (B) Representative gating of MHC-II and CD206 staining for identification of MHC-II+, CD206- (M1) and MHC-II-, CD206+(M2) macrophages. (C) Ratio of M2:M1 macrophages in 3LL tumors at day 17 (n = 7-12) pooled from two experiments. (D-E) MHC II MFI expression of 3LL tumor associated macrophages (TAMs) pooled from two experiments (n = 7-13). (F) Percent CD3 of CD45+ Live cells within the tumor of untreated and anti-PD-1 treated mice for male and female mice both lean/DIO (n = 3-4), representative of at least two independent experiments. (G) Volcano plot illustrating differentially expressed genes from bulk RNAseq of 3LL tumors between male and female DIO mice (H-I) Highlighted genes associated with macrophage polarization (H) M1 and (I) M2 from bulk RNAseq of 3LL tumors significant by adjusted p value. One way ANOVA with multiple comparisons was utilized for (A, C, E, and F).

Figure 4. Metabolomic profiling reveals links across species in obesity and identifies distinctions based on sex. (A) Metabolomic analysis from a small study of serum obtained from 5 normal BMI (BMI < 25, blue) and 3 obese (BMI ≥30, purple) individuals, treated with immunotherapy were found to either have stable disease (orange), progressive disease (pink), or hyperprogressive disease (green). (B-E) Volcano plots illustrating differentially abundant metabolites from serum metabolomics analysis on C57BL/6 mice (B) male lean vs. DIO, (C) female lean vs. DIO, (D) female leans vs male lean, and (E) female DIO vs male DIO. (F-G) Violin plots depicting metabolites shared with human obesity signature that are (F) increased in human obesity and significantly more abundant in DIO males over DIO females, (G) decreased in human obesity and significantly more abundant in DIO females over DIO males. One way ANOVA with multiple comparisons was utilized for (F-G).

Figure 5. Prior-ovariectomy (OVX) restores the immunotherapy response in DIO female mice and mediates changes in hormonal profile. (A) Schema depicting C57BL/6 male, female and ovariectomized female mice placed on 10% and 60% fat diet regimen over the course of 16 weeks and subsequently challenged with subcutaneous B16F0 or 3LL tumors. (B-C) Tumor growth curves of male, female and OVX DIO C57BL/6 mice challenged with (B) B16F0 and (C) 3LL subcutaneously and treated with either a regimen of anti-PD-1 or isotype control (n = 6-8) each representative of at least two experiments. (D-E) Waterfall plots illustrating change in tumor volume of anti-PD-1 treated lean and DIO mice (male, female, and OVX) graphed as change in tumor volume from isotype controls. (F) Representative gating of MHC-II and CD206 staining for identification of MHC-II+, CD206- (M1) and MHC-II-, CD206+(M2) macrophages of DIO mice. (G) MHC II percent positive tumor associated macrophages (TAMs) and (H) ratio of M2:M1 TAMs in 3LL tumors of DIO male, female, and OVX at day 17 (n = 5-8). (I-J) Percentage of infiltrating CD8 and CD4 T cells of total CD45+ live cells assed via flow cytometry in 3LL tumors of DIO male, female, and OVX at day 17 (n = 3-4) representative of two independent experiments. Two-way ANOVA with multiple comparisons was used for analysis of (B, C) One way ANOVA with multiple comparisons was utilized for (G-K, M).

Figure 6. Stratification of female patients by age and BMI reveals distinctions in immunotherapy outcomes. (A) Kaplan-Meier estimates of overall survival of 136 female patients stratified by age (< 55 [LT] or ≥ 55 [GTE]) and obesity status (BMI < 30 [LT] of BMI ≥ 30 [GTE]) using product-limit survival estimates with number of patients at risk. (B) M2 macrophages CIBERSORT Immune deconvolution signature utilizing lung cancer data from the cancer Genome Atlas (TCGA) grouped on male, pre-menopausal (age <55), and post-menopausal women (age ≥ 55) (n =46- 256) using a one-way ANOVA with Sidak's multiple comparison test.

Figure 7. Metabolomic signatures linking DIO male and ovariectomized females is associated with immunotherapy responses. (A) Principal component analysis (PCA) of serum metabolomics grouped by lean or DIO phenotype and sex. (B) Heatmap of top differentially abundant metabolites between lean male, female and ovariectomized female (OVX) concurrent with DIO male, female and OVX (metabolites in order from top: TG(18:0_38:6), TG(20:5_36:3), TG(18:2_38:4), TG(18:2_38:6), TG(16:0_40:8), TG(18:2_38:5), TG(20:4_36:3), TG(20:4_36:4), TG(18:0_36:2), TG(18:1_36:0), TG(17:0_36:3), DG(18:1_18:2), DG(16:0_18:2), TG(22:4_34:2), TG(20:4_34:3), TG(16:0_38:6), TG(20:4_34:2), TG(20:4_34:1), TG(22:5_34:1), TG(16:0_34:1), TG(20:2_34:1), TG(20:2_34:2),1-Met-His, SM C16:1, SM C24:0, PC aa C34:1, PC aa C32:0, SM C24:1, PC aa C38:6, PC aa C36:4, PC aa C38:1. PC ae C38:0, PC aa C32:1, CE(16:1), lysoPC a C16:1, TG(16:1_36:2), TG(18:1_32:1), TG(16:1_34:1), TG(16:1_34:2), TG(16:1_32:1), TG(16:1_34:3), DG(18:1_18:1), DG(16:1_18:1), Met-SO, TG(20:3_32:0), SM (OH) C16.1, Cer(d18.1/19:0), SM C16:0, SM C18:1, SM C18:0, TG(18:3_38:5), PC aa C36:2, CE(18:2), TG(18:1_36:1), TG(20:1_34:0), TMAO, MET, Lys, Thr, Tyr, Val, Kynurenine, HipAcid, Carnosine, Harg, C0, PC aa C30:0, TG(14:0_35:1), TG(17:2_36:2), Cer(d18:1/20:0(OH)), PC aa C36:0, SM C22:3, TG(20:4_35:3), SM C20:2, PC aa C32:3. (C) Venn diagrams illustrating differentially increased and decreased metabolites in obesity and similarities based on sex and ovariectomy. (D-F) Volcano pots depicting differentially abundant metabolites between (D) lean and DIO OVX, (E) DIO OVX and DIO male, and (F) DIO OVX and DIO female groups. (G-I) Scatterplots depicting correlations of metabolite quantitation of PC aa 36:2 (G), PC aa C38:4 (H), and AABA (I) with changes in tumor volume following anti-PD-1 treatment in DIO mice challenged with 3LL tumors. Simple linear regressions were utilized for G-I.

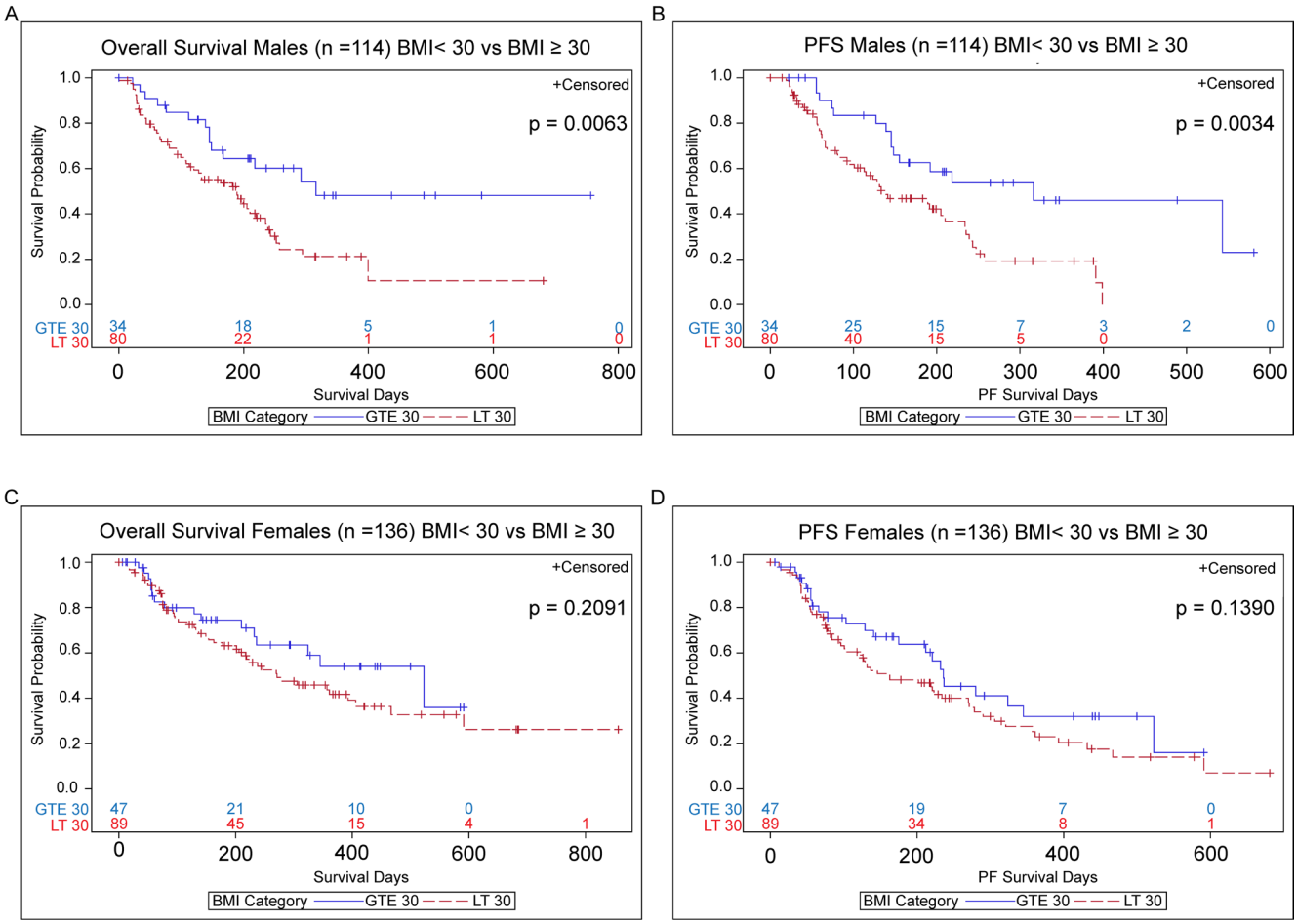


Figure 1. Obesity is associated with better outcomes in male, but not female patients receiving immune checkpoint inhibitors. (A-B) Kaplan-Meier estimates (product-limit survival estimates) with number of patients at risk of overall survival and progression free survival of 114 male and (C-D) 136 female patients receiving PD-1/L1 ICI stratified based on BMI < 30 (LT) or ≥ 30 (GTE) (n =114, 136).

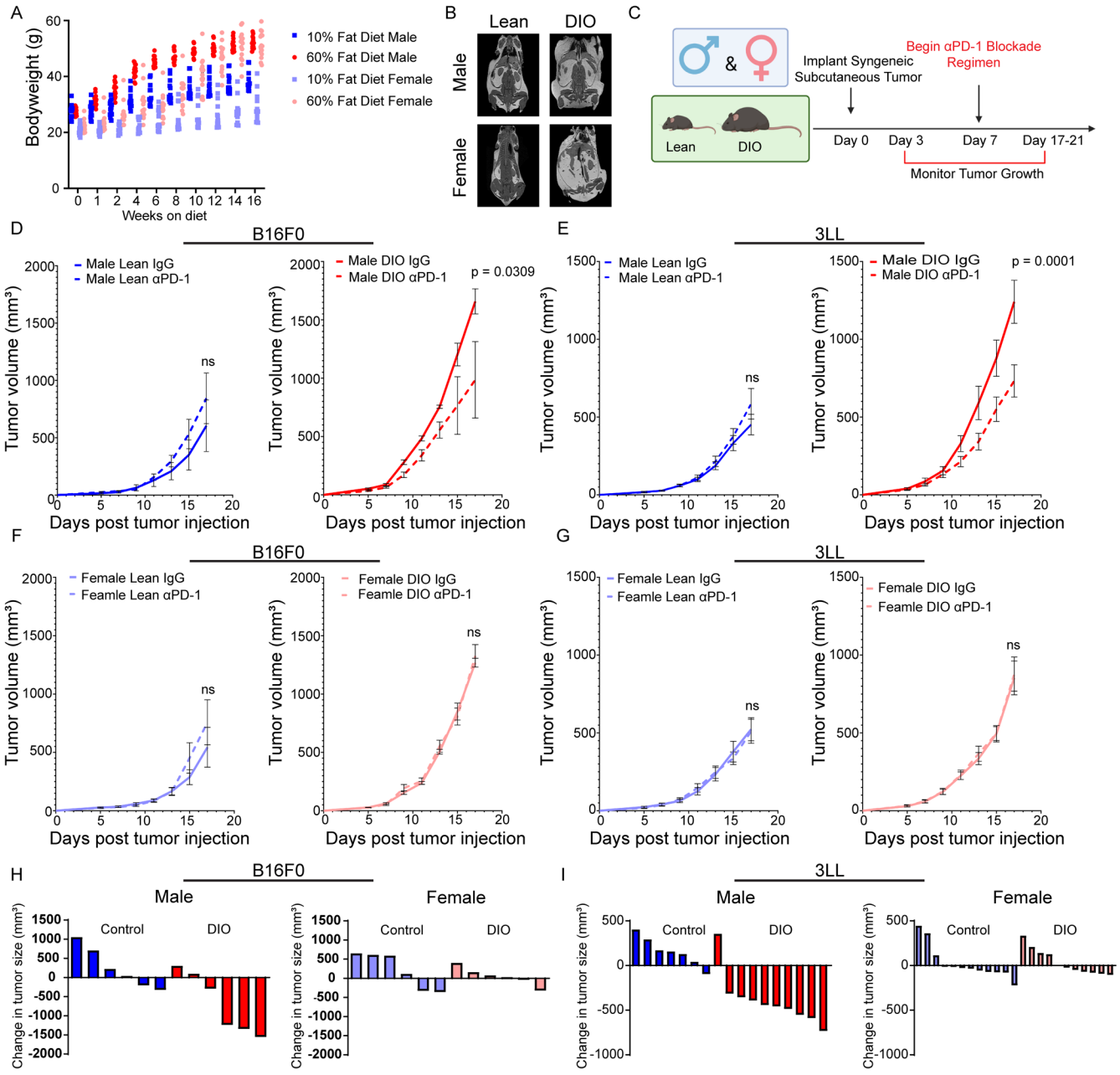


Figure 2: **Male but not female DIO mice demonstrate decreased tumor burden and improved anti-tumor responses following anti-PD-1 immunotherapy.** (A) Weight (grams) of C57BL/6 mice over the course of diet regimen (n =19-20). Data representative of at least four cohorts/experiments. (B) Magnetic resonance images of lean and DIO male and female mice post diet regimen. (C) Schema detailing experimental design of lean and DIO mice implanted with subcutaneous tumors and treated with anti-PD-1 or isotype control until tumor assessment. (D-E) Tumor growth curves of untreated lean and DIO mice grouped by sex implanted subcutaneously with syngeneic tumor lines (D-E) B16F0 (n =4-6) a single experiment representative of 3 independent experiments and (F-G) 3LL (n = 11-12) data pooled from two experiments representative of 5 independent experiments. (H-I) Waterfall plots depicting change in tumor volume of anti-PD-1 treated mice from corresponding controls for male and female lean/DIO C57BL/6 mice implanted with (H)B16F0 & (I) 3LL (n = 5 - 12). Two-way ANOVA with multiple comparisons was used for analysis of (D-E and H-I), ns: not significant, $p \leq 0.05$.

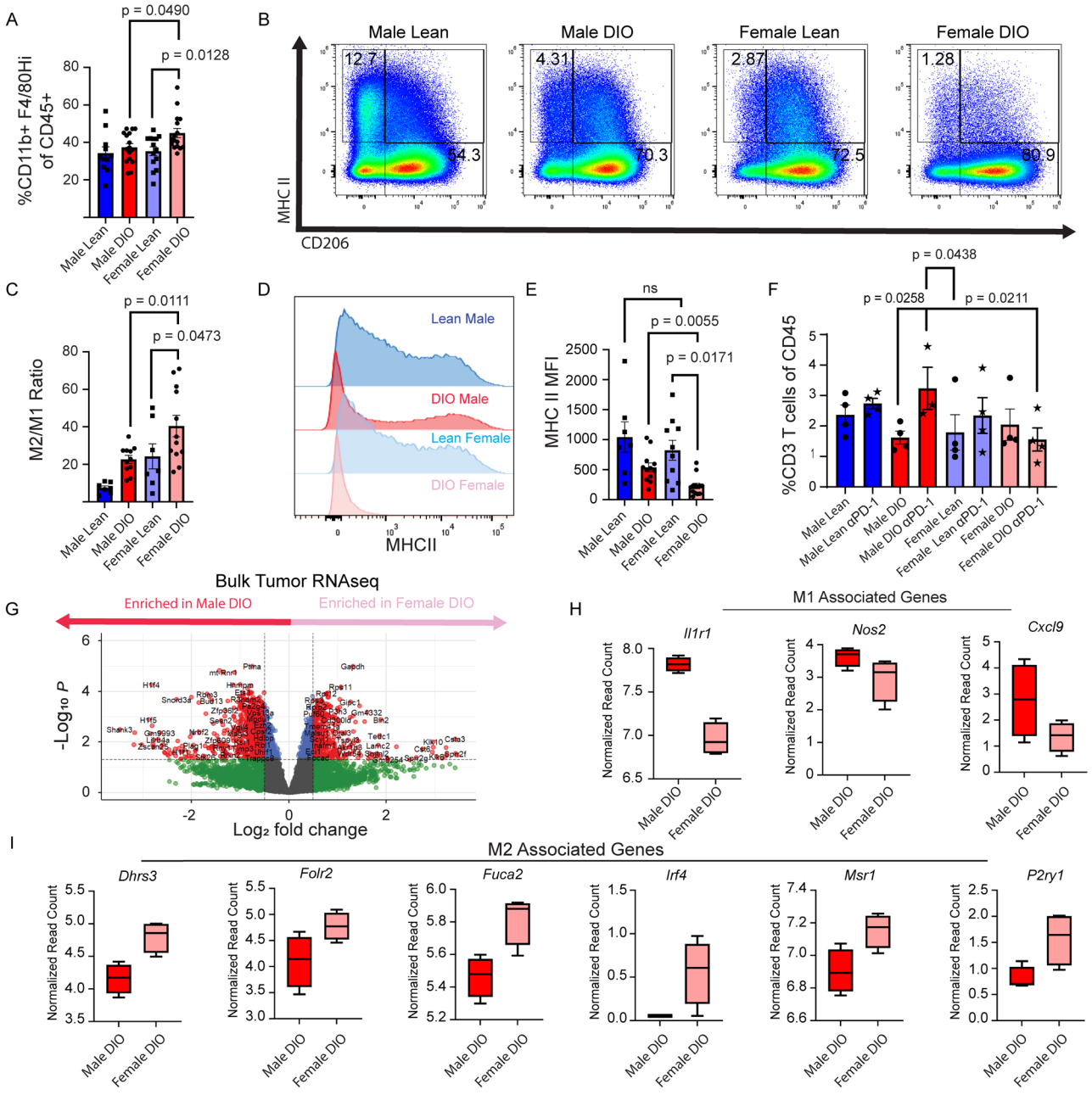


Figure 3. Obesity differentially modulates the tumor microenvironment based on biologic sex promoting increased M2 tumor associated macrophages in DIO female mice. (A) Quantified percentages of CD11b+F4/80Hi cells of live CD45+ cells in 3LL tumors from lean and DIO mice of both sexes, pooled from three experiments (n = 11-17). (B) Representative gating of MHC-II and CD206 staining for identification of MHC-II+, CD206- (M1) and MHC-II-, CD206+(M2) macrophages. (C) Ratio of M2:M1 macrophages in 3LL tumors at day 17 (n = 7-12) pooled from two experiments. (D-E) MHC II MFI expression of 3LL tumor associated macrophages (TAMs) pooled from two experiments (n = 7-13). (F) Percent CD3 of CD45+ Live cells within the tumor of untreated and anti-PD-1 treated mice for male and female mice both lean/DIO (n = 3-4), representative of at least two independent experiments. (G) Volcano plot illustrating differentially expressed genes from bulk RNAseq of 3LL tumors between male and female DIO mice (H-I) Highlighted genes associated with macrophage polarization (H) M1 and (I) M2 from bulk RNAseq of 3LL tumors significant by adjusted p value. One way ANOVA with multiple comparisons was utilized for (A, C, E, and F).

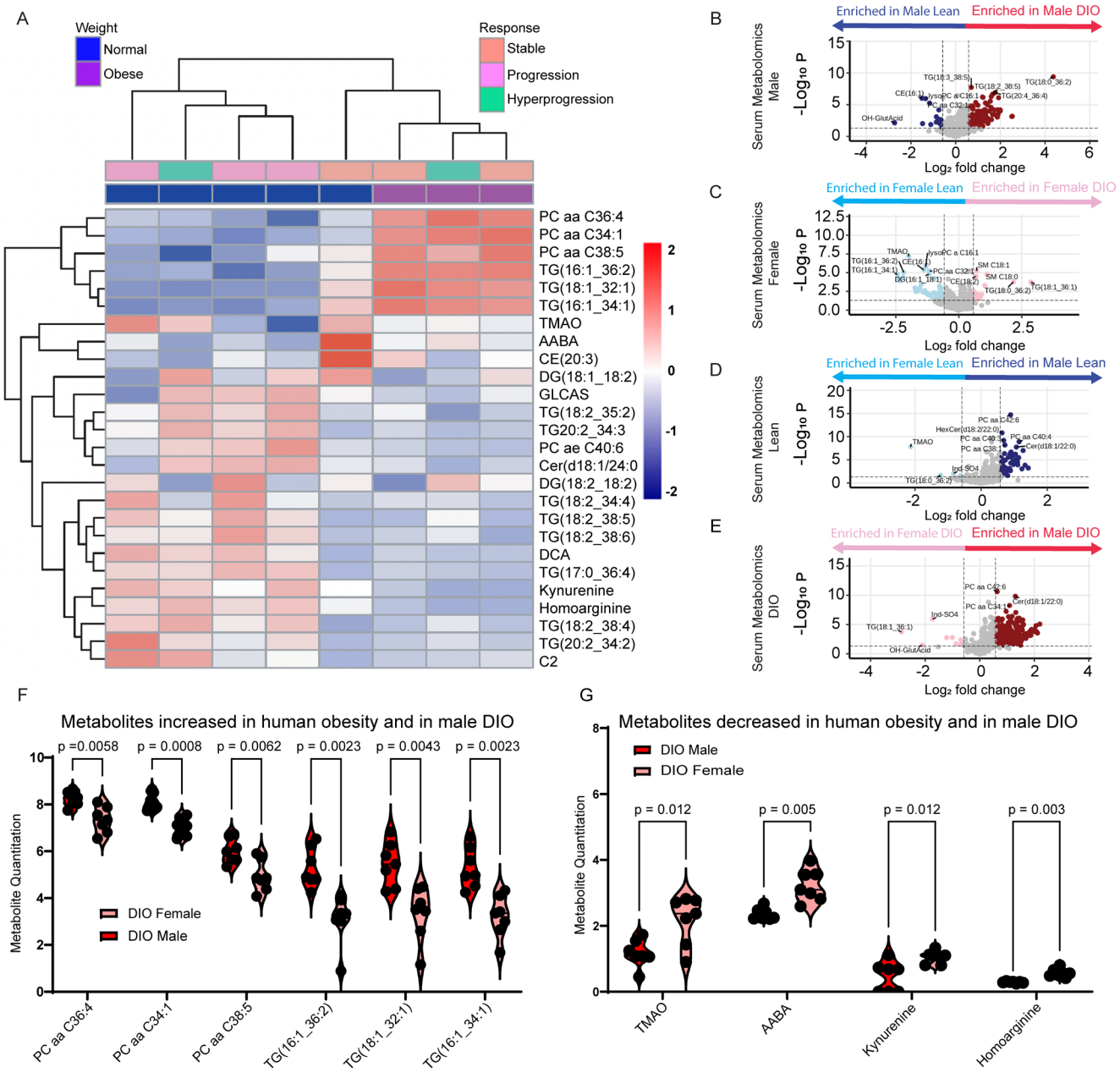


Figure 4. Metabolomic profiling reveals links across species in obesity and identifies distinctions based on sex. (A) Metabolomic analysis from a small study of serum obtained from 5 normal BMI (BMI < 25, blue) and 3 obese (BMI ≥30, purple) individuals, treated with immunotherapy were found to either have stable disease (orange), progressive disease (pink), or hyperprogressive disease (green). (B-E) Volcano plots illustrating differentially abundant metabolites from serum metabolomics analysis on C57BL/6 mice (B) male lean vs. DIO, (C) female lean vs. DIO, (D) female leans vs male lean, and (E) female DIO vs male DIO. (F-G) Violin plots depicting metabolites shared with human obesity signature that are (F) increased in human obesity and significantly more abundant in DIO males over DIO females, (G) decreased in human obesity and significantly more abundant in DIO females over DIO males. One way ANOVA with multiple comparisons was utilized for (F-G).

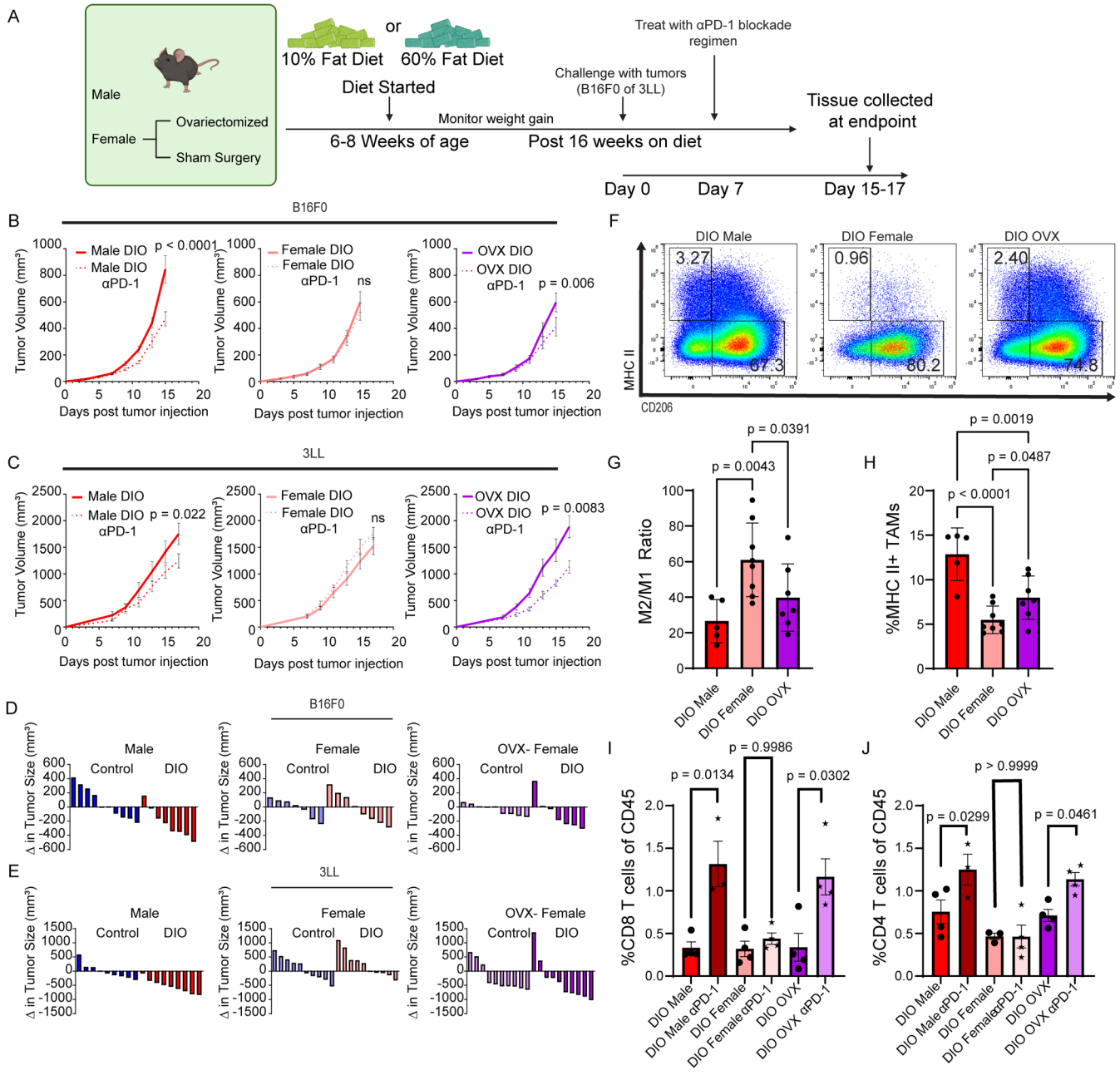


Figure 5. Prior-ovariectomy (OVX) restores the immunotherapy response in DIO female mice and mediates changes in hormonal profile. (A) Schema depicting C57BL/6 male, female and ovariectomized female mice placed on 10% and 60% fat diet regimen over the course of 16 weeks and subsequently challenged with subcutaneous B16F0 or 3LL tumors. (B-C) Tumor growth curves of male, female and OVX DIO C57BL/6 mice challenged with (B) B16F0 and (C) 3LL subcutaneously and treated with either a regimen of anti-PD-1 or isotype control (n = 6-8) each representative of at least two experiments. (D-E) Waterfall plots illustrating change in tumor volume of anti-PD-1 treated lean and DIO mice (male, female, and OVX) graphed as change in tumor volume from isotype controls. (F) Representative gating of MHC-II and CD206 staining for identification of MHC-II+, CD206- (M1) and MHC-II-, CD206+(M2) macrophages of DIO mice. (G) MHC II percent positive tumor associated macrophages (TAMs) and (H) ratio of M2:M1 TAMs in 3LL tumors of DIO male, female, and OVX at day 17 (n = 5-8). (I-J) Percentage of infiltrating CD8 and CD4 T cells of total CD45+ live cells assed via flow cytometry in 3LL tumors of DIO male, female, and OVX at day 17 (n = 3-4) representative of two independent experiments. Two-way ANOVA with multiple comparisons was used for analysis of (B, C) One way ANOVA with multiple comparisons was utilized for (G-J).

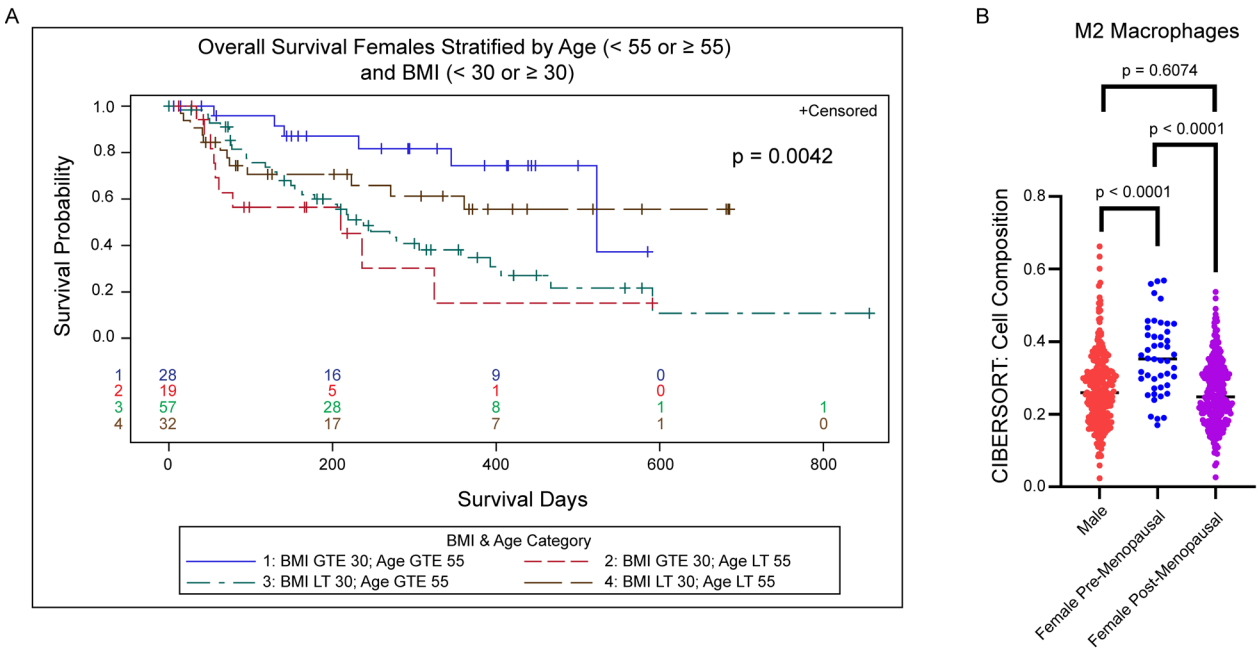


Figure 6. Stratification of female patients by age and BMI reveals distinctions in immunotherapy outcomes. (A) Kaplan-Meier estimates of overall survival of 136 female patients stratified by age (< 55 [LT] or ≥ 55 [GTE]) and obesity status (BMI < 30 [LT] of BMI ≥ 30 [GTE]) using product-limit survival estimates with number of patients at risk. (B) M2 macrophages CIBERSORT Immune deconvolution signature utilizing lung cancer data from the cancer Genome Atlas (TCGA) grouped on male, pre-menopausal (age <55), and post-menopausal women (age ≥ 55) (n =46 - 256) using a one-way ANOVA with Sidak's multiple comparison test.

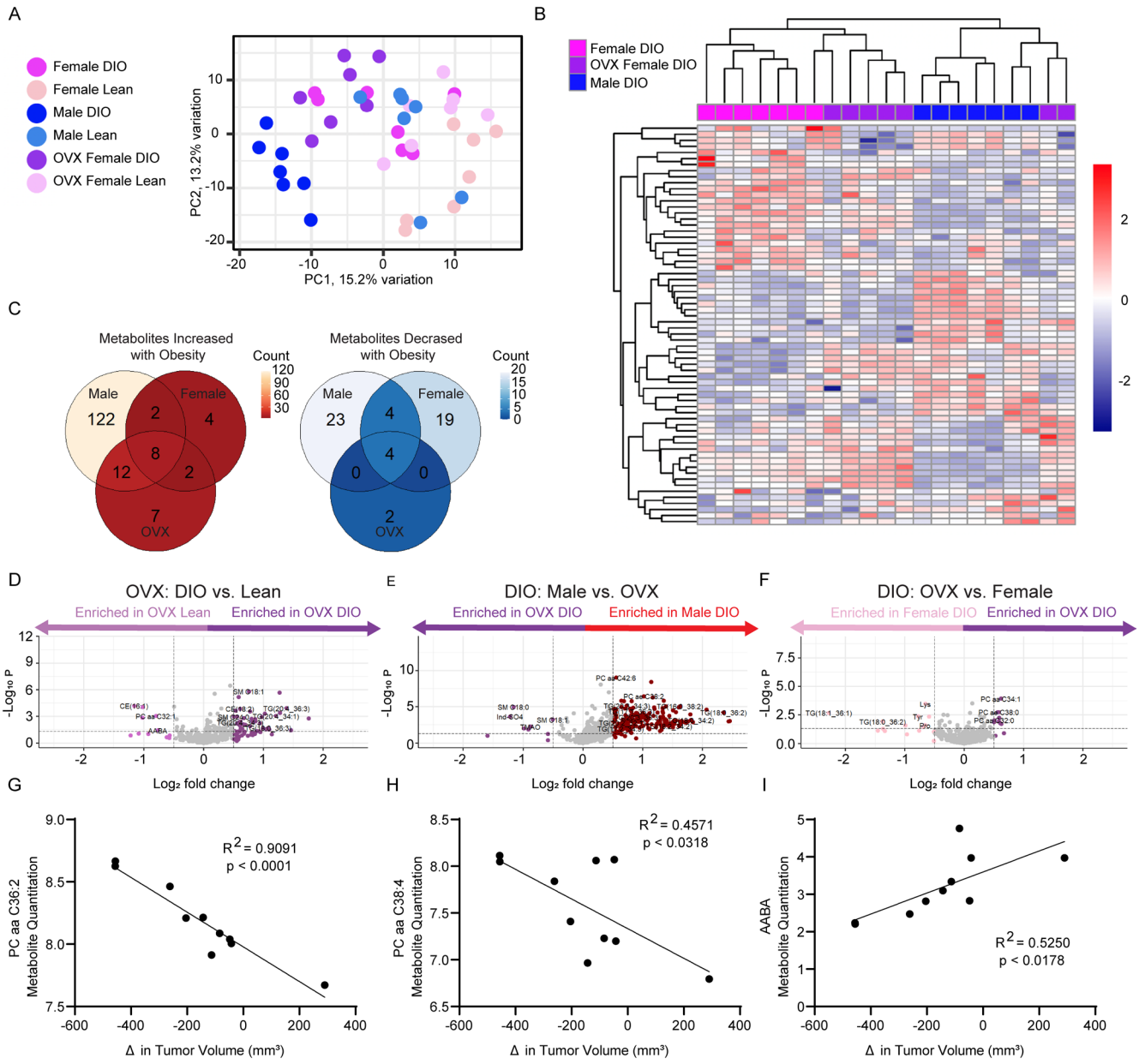


Figure 7. Metabolomic signatures linking DIO male and ovariectomized females is associated with immunotherapy responses. (A) Principal component analysis (PCA) of serum metabolomics grouped by lean or DIO phenotype and sex. (B) Heatmap of top differentially abundant metabolites between lean male, female and ovariectomized female (OVX) concurrent with DIO male, female and OVX (metabolites in order from top: TG(18:0_38:6), TG(20:5_36:3), TG(18:2_38:4), TG(18:2_38:6), TG(16:0_40:8), TG(18:2_38:5), TG(20:4_36:3), TG(20:4_36:4), TG(18:0_36:2), TG(18:1_36:0), TG(17:0_36:3), DG(18:1_18:2), DG(16:0_18:2), TG(22:4_34:2), TG(20:4_34:3), TG(16:0_38:6), TG(20:4_34:2), TG(20:4_34:1), TG(22:5_34:1), TG(16:0_34:1), TG(20:2_34:1), TG(20:2_34:2),1-Met-His, SM C16:1, SM C24:0, PC aa C34:1, PC aa C32:0, SM C24:1, PC aa C38:6, PC aa C36:4, PC aa C38:1. PC ae C38:0, PC aa C32:1, CE(16:1), lysoPC a C16:1, TG(16:1_36:2), TG(18:1_32:1), TG(16:1_34:1), TG(16:1_34:2), TG(16:1_32:1), TG(16:1_34:3), DG(18:1_18:1), DG(16:1_18:1), Met-SO, TG(20:3_32:0), SM (OH) C16.1, Cer(d18.1/19:0), SM C16:0, SM C18:1, SM C18:0, TG(18:3_38:5), PC aa C36:2, CE(18:2), TG(18:1_36:1), TG(20:1_34:0), TMAO, MET, Lys, Thr, Tyr, Val, Kynurenine, HipAcid, Carnosine, Harg, C0, PC aa C30:0, TG(14:0_35:1), TG(17:2_36:2), Cer(d18:1/20:0(OH)), PC aa C36:0, SM C22:3, TG(20:4_35:3), SM C20:2, PC aa C32:3. (C) Venn diagrams illustrating differentially increased and decreased metabolites in obesity and similarities based on sex and ovariectomy. (D-F) Volcano pots depicting differentially abundant metabolites between (D) lean and DIO OVX, (E) DIO OVX and DIO male, and (F) DIO OVX and DIO female groups. (G-I) Scatterplots depicting correlations of metabolite quantitation of PC aa 36:2 (G), PC aa C38:4 (H), and AABA (I) with changes in tumor volume following anti-PD-1 treatment in DIO mice challenged with 3LL tumors. Simple linear regressions were utilized for (G-I).